

## Quantum phases of dipolar bosons in a multilayer optical lattice

Soumik Bandyopadhyay ,<sup>1,2,3</sup> Hrushikesh Sable ,<sup>1,2</sup> Deepak Gaur ,<sup>1,2</sup> Rukmani Bai ,<sup>1,4</sup> Subroto Mukerjee,<sup>5</sup> and D. Angom <sup>1,6</sup>

<sup>1</sup>Physical Research Laboratory, Ahmedabad - 380009, Gujarat, India

<sup>2</sup>Indian Institute of Technology Gandhinagar, Palaj, Gandhinagar - 382355, Gujarat, India

<sup>3</sup>INO-CNR BEC Center and Department of Physics, University of Trento, Via Sommarive 14, I-38123 Trento, Italy

<sup>4</sup>Institute for Theoretical Physics III and Center for Integrated Quantum Science and Technology, University of Stuttgart, 70550 Stuttgart, Germany

<sup>5</sup>Department of Physics, Indian Institute of Science, Bangalore - 560012, India

<sup>6</sup>Department of Physics, Manipur University, Canchipur - 795003, Manipur, India



(Received 3 November 2021; revised 6 July 2022; accepted 14 September 2022; published 3 October 2022)

We consider a minimal model to investigate the quantum phases of hardcore, polarized dipolar atoms confined in multilayer optical lattices. The model is a variant of the extended Bose-Hubbard model, which incorporates intralayer repulsion and interlayer attraction between the atoms in nearest-neighbor sites. We study the phases of this model emerging from the competition between the attractive interlayer interaction and the interlayer hopping. Our results from the analytical and cluster-Gutzwiller mean-field theories reveal that multimer formation occurs in the regime of weak intra- and interlayer hopping due to the attractive interaction. In addition, intralayer isotropic repulsive interaction results in the checkerboard ordering of the multimers. This leads to an incompressible checkerboard multimer phase at half-filling. At higher interlayer hopping, the multimers are destabilized to form resonating valence-bond-like states. Furthermore, we discuss the effects of thermal fluctuations on the quantum phases of the system.

DOI: [10.1103/PhysRevA.106.043301](https://doi.org/10.1103/PhysRevA.106.043301)

### I. INTRODUCTION

The experimental demonstration of the superfluid to Mott-insulator phase transition in the 1D, 2D and 3D optical lattices with bosonic atoms [1–6] marks a paradigm shift in the exploration of quantum phase transitions. High tunability of the system parameters and almost near complete isolation of ultracold atoms in the optical lattice potentials have thus opened a new avenue to explore quantum many-body physics [7–9]. At present, optical lattices are considered as macroscopic quantum simulators of condensed matter systems [10,11]. They have been employed to understand properties of equilibrium quantum phases [12–20], characteristics of collective excitations [21–26], nonequilibrium dynamics of quantum phase transitions [27–33], quantum thermalization [34,35], the many-body localization transition [36,37], driven and dissipative dynamics [38,39], etc. Optical lattices, when loaded with Bose-Einstein condensed atoms, can simulate the Bose-Hubbard model (BHM) [12,40]. This model is the bosonic counterpart of the Hubbard model [41]. The latter has been considered as the prototypical model to understand the properties of interacting electrons in the tight binding regime. The BHM considers only nearest-neighbor hopping and onsite contact interaction. These basic considerations are sufficient to describe the properties of the superfluid and Mott insulator phases of neutral atoms. But, BHM can not describe phases arising from the long-range interatomic interactions.

A minimal extension of the BHM includes nearest-neighbor (NN) interactions. The model is, then, referred to as the extended BHM. Several theoretical studies have analyzed

the quantum phases of this model [19,42–47]. This interaction can induce periodic density modulation, which is a type of diagonal order. The system can also host a supersolid, which is characterized by the coexistence of diagonal and off-diagonal long-range order, and has been a topic of extensive research [48]. The extended BHM has been experimentally realized in a 3D optical lattice loaded with magnetic dipolar atoms [6]. However, to be precise, the interatomic dipole-dipole interaction is long-range and anisotropic. Consequently, several theoretical studies have investigated the effects of these features on the quantum phases [13–17,49,50], leading to a further generalization of BHM. In this context, the dimensionality of the lattice plays an important role. For example, for dipoles polarized perpendicular to the lattice plane, the intralayer NN interaction is repulsive and isotropic. However, the interlayer NN interaction is attractive. Such an anisotropy can stabilize additional quantum phases in a 3D system. A simplified or minimal 3D lattice system is stacking two layers of a 2D lattice. While with the increase in number of layers, 3D properties of the system become more prominent.

Recent observations of unconventional superconductivity [51] and correlated insulating phase [52] in twisted bilayer graphene have provided an impetus for studies on bilayer systems [53–58]. There are proposals to simulate the physics of twisted bilayers using optical lattice setups [56,59]. Furthermore, the bilayer continuum and lattice systems with polarized dipolar atoms [60–64], can host a multitude of quantum phases, which are absent in monolayer. In particular, due to the attractive interlayer interaction, there can be a pairing between the atoms in the different layers. Then, lattice sys-

tems can host phases like the pair superfluid [60,62,63], pair supersolid [62,63], etc. However, the interlayer hopping can destabilize the pairs, and lead to the formation of phases like the valence bond solid and supersolid [64].

In this work, we investigate the quantum phases of polarized dipolar atoms confined to a multilayer optical lattice. In particular, we focus on bi- and trilayer lattices. We study the ground state quantum phases of the system using the cluster Gutzwiller mean-field theory [65–69]. Our study reveals the existence of exotic quantum phases arising from the competitions of the intra- and interlayer interactions and hoppings. This study encapsulates one of the important aspects of the multilayer systems by varying the interlayer hopping from the weak to the strong domain. We supplement the numerical phase boundaries between the incompressible and compressible phases through an analytical approach based on mean-field perturbation theory. Unlike earlier studies based on the site-decoupling scheme [17,70–72], here we include the interlayer hopping in the unperturbed Hamiltonian and apply the method with respect to multiple sites. This approach can be thought of as a cluster generalization of the site-decoupling method. Furthermore, we extend our study to the finite temperature domain in order to understand the stability of quantum phases against thermal fluctuations. Probing the novel quantum phases of quintessential models in condensed matter and quantum many-body systems has been one of the key motivations of quantum simulation [7–11]. One recent development which has a direct bearing on this is the experimental achievement of 3D optical lattice with long-range interactions using Erbium atoms [6] to probe MI and SF phases. Other related developments are the experimental studies on multilayer optical lattice systems with ultracold atoms [73–75]. The structured incompressible quantum phases reported in this work are in the strongly interacting regime and require temperatures below 1 nK to observe them. Although reaching such temperatures with dipolar atomic gases is challenging at present, we expect that with novel cooling techniques, it would be possible in the future experiments. Therefore the results presented in this manuscript shall be valuable to the future experiments in providing detailed information about the parameter domains of the novel quantum phases of dipolar atoms in multilayer optical lattices.

We have organized the remainder of this paper as follows. In Sec. II, we discuss the extended BHM apt for a description of polarized dipolar atoms in multilayers of 2D square optical lattice. In Secs. III A–III C, we give a brief account of the cluster Gutzwiller mean-field theory, adapted numerical procedure to solve the model, and the quantum phases of the system. In Sec. III D, we discuss the mean-field perturbation analysis to obtain analytical phase boundaries between incompressible and compressible phases. In Sec. IV, we present and elaborate the phase diagrams of the bi- and trilayer lattice systems and then discuss the effects of finite temperature on the quantum phases. In Sec. V, we summarize our key results and conclude.

## II. THEORETICAL MODEL

We consider polarized dipolar atoms confined to bi- and trilayers of a two-dimensional (2D) square optical lattice [6, 13–17] with in-plane lattice constant  $a$ . The  $x$  and  $y$  coordi-

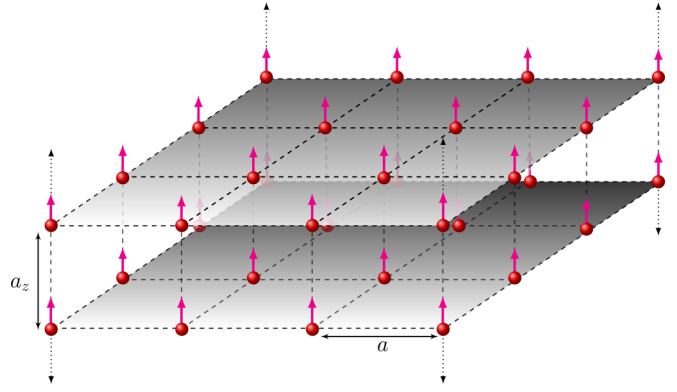


FIG. 1. Schematic representation of the dipolar bosonic atoms in a bilayer optical lattice. The lattice spacing within a layer is  $a$ , and interlayer spacing is  $a_z$ . The red spheres represent atoms, and the arrows indicate the orientation of the dipole. The dotted arrows indicate possible extension to multilayered optical lattice.

inates of the lattice sites with index  $i \equiv (p, q)$  in layers 1, and 2 (and 3) coincide, but, these lattice sites are separated by a distance  $a_z$  along the  $z$  direction as shown in Fig. 1. So, in general, the unit cell of the multilayer lattice system is a cuboid and cube for the special case of  $a_z = a$ . For the polarized dipolar atoms, the dipole-dipole interaction potential is

$$U_{dd} = C_{dd} \frac{(1 - 3\cos^2\alpha)}{|\vec{R} - \vec{R}'|^3}, \quad (1)$$

where,  $C_{dd}$  is the dipolar interaction strength,  $\alpha$  is the angle between the polarization axis and the separation vector ( $\vec{R} - \vec{R}'$ ). In the square lattice, the position vector of a site is  $\vec{R} \equiv a(p\hat{e}_x + q\hat{e}_y) + a_z r\hat{e}_z$ , where  $p, q, r \in \mathbb{Z}$ .

The dipolar interaction strength between two lattice sites is determined by the overlap between the lowest Bloch-band Wannier functions and it decreases exponentially as the intersite separation is increased. Hence, approximating the long-range dipolar interaction with NN interaction provides a good qualitative description of the quantum phases supported by the system [6,76]. So in the present study, we limit the range of the dipole-dipole interaction to the NN sites [17,19], and consider the dipole moments of the atoms to be oriented along the  $z$  axis. Then, from Eq. (1) it is evident that the intralayer NN dipole-dipole interaction is repulsive and isotropic. The interlayer NN interaction is, however, attractive. For compact notations, let us denote the strengths of the intralayer and interlayer NN interactions by  $V \propto d^2/a^3$  and  $V' \propto 2d^2/a_z^3$ , respectively, where  $d$  is the magnitude of the induced dipole moment.

In addition, we consider the atoms to be hardcore, that is, not more than one atom can occupy each site of the lattice. This is the case when the onsite repulsive interatomic interaction energy is much larger than other energy scales: hopping and dipole-dipole interaction energies. This, then, energetically favors single occupancy and atoms can be treated as hardcore bosons. So, the local Fock space has dimension  $N_b = 2$  with basis states  $|0\rangle$  and  $|1\rangle$  corresponding to zero and single occupation at a site, respectively. Then, the grand-canonical

Hamiltonian describing the bilayer system is

$$\begin{aligned} \hat{H}_{\text{bi}} = & -J \sum_{(ij),r} (\hat{b}_{i,r}^\dagger \hat{b}_{j,r} + \text{H.c.}) - J' \sum_i (\hat{b}_{i,1}^\dagger \hat{b}_{i,2} + \text{H.c.}) \\ & + V \sum_{(ij),r} \hat{n}_{i,r} \hat{n}_{j,r} + V' \sum_i \hat{n}_{i,1} \hat{n}_{i,2} - \mu \sum_{i,r} \hat{n}_{i,r}, \end{aligned} \quad (2)$$

where  $r \in \{1, 2\}$  is the layer index;  $\hat{b}_{i,r}^\dagger$ ,  $\hat{b}_{i,r}$  and  $\hat{n}_{i,r}$  are the local bosonic creation, annihilation and occupation number operators. Here,  $J$  is the strength of intralayer hopping considered identical for all the layers,  $J'$  is the interlayer hopping strength, and  $\mu$  the chemical potential which fixes the total number of atoms in the system. It is important to note that the interlayer hopping strength can be varied by changing the depth of the optical lattice along  $z$  direction. In experiments, this is done by tuning the intensity of counterpropagating laser beams along the  $z$  direction [6]. To extend the model to a larger number of layers, define the Hamiltonian for one lattice plane as

$$\hat{H}_r = \sum_{(ij)} [-J(\hat{b}_{i,r}^\dagger \hat{b}_{j,r} + \text{H.c.}) + V \hat{n}_{i,r} \hat{n}_{j,r}] - \mu \sum_i \hat{n}_{i,r}, \quad (3)$$

then, the bilayer Hamiltonian in Eq. (2) assumes the form

$$\hat{H}_{\text{bi}} = \sum_{r=1}^2 \hat{H}_r - J' \sum_i (\hat{b}_{i,1}^\dagger \hat{b}_{i,2} + \text{H.c.}) + V' \sum_i \hat{n}_{i,1} \hat{n}_{i,2}. \quad (4)$$

The Hamiltonian can be generalized to the case of  $M$  layers as

$$\begin{aligned} \hat{H}_M = & \sum_{r=1}^M \hat{H}_r - J' \sum_i \sum_{r=1}^{M-1} (\hat{b}_{i,r}^\dagger \hat{b}_{i,r+1} + \text{H.c.}) \\ & + V' \sum_i \sum_{r=1}^{M-1} \hat{n}_{i,r} \hat{n}_{i,r+1}. \end{aligned} \quad (5)$$

The bilayer system with attractive interlayer NN interaction and suppressed interlayer hopping can exhibit the PSS phase [60,62,63]. In this case, the pair formation is between the atoms in two different layers, and the pairs hop around the lattice. In addition, the intralayer repulsive and isotropic NN interaction can induce checkerboard order in the system. Then, a bilayer optical lattice system of polarized dipolar bosons can simultaneously exhibit superfluidity of pairs and crystalline order, which corresponds to pair supersolid (PSS) phase [62,63]. With the increase in interlayer hopping, the enhanced interlayer kinetic energy destabilizes the pairs. However, the resonating particle pair states can be stabilized when the interlayer hopping is large [64]. So, the hardcore dipolar atoms in bilayer system can exhibit a triplet state of the form

$$|t_0\rangle_{p,q} = \frac{1}{\sqrt{2}}(|10\rangle_{p,q} + |01\rangle_{p,q}), \quad (6)$$

where  $|m_1 m_2\rangle_{p,q}$  denotes a dimer state with  $m_1$  and  $m_2$  atoms at lattice site  $(p, q)$  of first and second layers, respectively. This triplet state is the bosonic counterpart of the familiar valence bond antisymmetric singlet state of electrons. Such a state has been studied in the extended BHM for 1D lattice systems [77–81]. Like in the case of PSS, the attractive and

repulsive inter- and intralayer interactions can induce checkerboard order to the valence-bond-like states as well. Then, the ground state of the system is referred to as the valence bond checkerboard solid (VCBS). In addition, the ground state of the system can exhibit superfluidity and valence bond checkerboard order simultaneously, which is referred to as valence bond supersolid (VSS) phase. It is worth noting that the pair expectation calculated with respect to the triplet state in Eq. (6) is

$${}_{p,q}\langle t_0 | \hat{n}_{p,q,1} \hat{n}_{p,q,2} | t_0 \rangle_{p,q} = 0. \quad (7)$$

An important symmetry of the Hamiltonian in Eq. (2) is manifested through the particle-hole transformation of the creation and annihilation operators. This transformation leads to replacing the particle creation operator  $\hat{b}_{i,r}^\dagger$  by hole annihilation operator  $\hat{a}_{i,r}$ , and particle annihilation operator  $\hat{b}_{i,r}$  by hole creation operator  $\hat{a}_{i,r}^\dagger$  in the Hamiltonian. Then, by employing canonical anticommutation relations between these operators (details are in Appendix A), we obtain the particle-hole symmetry point along the  $\mu$  axis of the phase diagram as  $\mu = [4V + V']/2$  for a bilayer system.

### III. THEORETICAL METHODS

#### A. Cluster Gutzwiller mean-field theory

We solve the model using the cluster mean-field theory with Gutzwiller ansatz [17–19,40,82–85]. For this, we subdivide the  $K \times L \times M$  lattice system ( $K$  and  $L$  are the number of lattice sites along  $x$  and  $y$  directions) into  $W$  small clusters of  $k \times l \times m$  lattice sites, that is,  $W = (K \times L \times M)/(k \times l \times m)$ . Then, like in the site-decoupled mean-field theory, we can define a local Hamiltonian of the clusters [18,19,69,84], and the total Hamiltonian is the sum of the cluster Hamiltonians.

In the present work, we limit ourselves to the case of bilayer ( $M = 2$ ) and trilayer ( $M = 3$ ) systems. The Hamiltonian of a cluster in the bilayer system is

$$\begin{aligned} \hat{H}_C = & \sum_r \left\{ \sum'_{p,q \in C} [-J(\hat{b}_{p+1,q,r}^\dagger \hat{b}_{p,q,r} + \hat{b}_{p,q+1,r}^\dagger \hat{b}_{p,q,r} \right. \\ & + \text{H.c.}) + V(\hat{n}_{p+1,q,r} \hat{n}_{p,q,r} + \hat{n}_{p,q+1,r} \hat{n}_{p,q,r})] \\ & + \sum_{p,q \in \delta C} [-J(\phi_{p+1,q,r}^* \hat{b}_{p,q,r} + \phi_{p,q+1,r}^* \hat{b}_{p,q,r} + \text{H.c.}) \\ & + V(\langle \hat{n}_{p+1,q,r} \rangle \hat{n}_{p,q,r} + \langle \hat{n}_{p,q+1,r} \rangle \hat{n}_{p,q,r})] \\ & \left. - \mu \sum_{p,q \in C} \hat{n}_{p,q,r} \right\} - \sum_{p,q \in C} [-J'(\hat{b}_{p,q,1}^\dagger \hat{b}_{p,q,2} + \text{H.c.}) \\ & + V' \hat{n}_{p,q,1} \hat{n}_{p,q,2}], \end{aligned} \quad (8)$$

where the prime in the summation denotes sum over lattice sites  $(p, q) \in C$ , such that,  $(p+1, q)$  and  $(p, q+1) \in C$ , and  $(p, q) \in \delta C$  denote the lattice sites at the boundary of the cluster  $C$ . The mean-field  $\phi_{p+1,q,r}^* = \langle \hat{b}_{p+1,q,r}^\dagger \rangle$  and average occupancy  $\langle \hat{n}_{p+1,q,r} \rangle$  with  $(p+1, q) \notin C$  are computed at the boundary of the neighboring cluster along  $x$ -direction, and are required to describe the intercluster hopping and NN interaction, respectively. Similarly,  $\phi_{p,q+1,r}^* = \langle \hat{b}_{p,q+1,r}^\dagger \rangle$  and  $\langle \hat{n}_{p,q+1,r} \rangle$  with  $(p, q+1) \notin C$  are required to describe the

intercluster hopping and NN interaction along  $y$  direction between adjacent clusters. Thus, within a cluster the hopping and NN interaction terms are exact, and the intercluster hopping and NN interactions are accounted through the mean-fields and average occupancies, respectively. It is important to note that the interlayer hopping and NN interaction terms are exact in the cluster Hamiltonian. Now, like in the site-decoupled mean-field theory, the cluster Hamiltonian matrix can be calculated using the Fock basis states of the cluster  $\{|n_0 n_1 \dots n_{m'}\rangle\}$ , where  $m' = (k \times l \times m) - 1$ . So, these basis states are the direct products of the local Fock states of the  $(k \times l \times m)$  lattice sites within the cluster. By diagonalizing the Hamiltonian matrix, the ground state of the cluster can be obtained in the form

$$|\psi_\alpha^C\rangle = \sum_{n_0 n_1 \dots n_{m'}} c_{n_0 n_1 \dots n_{m'}}^{(\alpha)} |n_0 n_1 \dots n_{m'}\rangle, \quad (9)$$

where  $\alpha$  is the cluster index, and  $c_{n_0 n_1 \dots n_{m'}}^{(\alpha)}$  are the complex coefficients of the ground state  $|\psi_\alpha^C\rangle$ . Then, employing the Gutzwiller ansatz, the ground state of the entire lattice is

$$|\Psi_{\text{GW}}\rangle = \prod_{\alpha=1}^W |\psi_\alpha^C\rangle = \prod_{\alpha=1}^W \sum_{n_0 n_1 \dots n_{m'}} c_{n_0 n_1 \dots n_{m'}}^{(\alpha)} |n_0 n_1 \dots n_{m'}\rangle. \quad (10)$$

The local superfluid order parameter and average occupancy at the  $(p, q)$  lattice site of the  $r$ th layer are

$$\begin{aligned} \phi_{p,q,r} &= \langle \Psi_{\text{GW}} | \hat{b}_{p,q,r} | \Psi_{\text{GW}} \rangle, \\ n_{p,q,r} &= \langle \Psi_{\text{GW}} | \hat{n}_{p,q,r} | \Psi_{\text{GW}} \rangle. \end{aligned} \quad (11)$$

A relevant parameter of a quantum phase is the average occupancy per lattice site,

$$\rho = \frac{1}{(K \times L \times M)} \sum_{p=1, q=1, r=1}^{K,L,M} n_{p,q,r}. \quad (12)$$

In this work, we study quantum phases with the hard-core approximation. So, we have  $\rho \leq 1$ . To probe the emergence of valence bond order in the bilayer system, we use the pair occupancy

$$\tilde{\rho}_{p,q} = \langle \Psi_{\text{GW}} | \hat{n}_{p,q,1} \hat{n}_{p,q,2} | \Psi_{\text{GW}} \rangle. \quad (13)$$

This quantity is zero when the triplet state, given in Eq. (6), is stabilized at the  $(p, q, 1)$  and  $(p, q, 2)$  sites of the bilayer system. It is also zero when atleast one of these sites is empty. It is nonzero only when both the sites are occupied, thereby exhibiting a pair. Thus,  $\tilde{\rho}_{p,q}$  along with  $n_{p,q,1}$  and  $n_{p,q,2}$  can identify the valence bond order in the system. And, the signatures of the triplet state are zero  $\tilde{\rho}_{p,q}$ , and finite  $n_{p,q,1}$  and  $n_{p,q,2}$ . The zero superfluid order parameter indicates the incompressibility of these solid phases and the checkerboard order in each layer is identified by the structure factor

$$S_r(\pi, \pi) = \frac{1}{K \times L} \sum_{\substack{p', q' \\ p, q}} e^{i\pi \{(p-p') + (q-q')\}} \langle \hat{n}_{p,q,r} \hat{n}_{p',q',r} \rangle. \quad (14)$$

In the phases with checkerboard order  $S_r(\pi, \pi)$  is finite, while it is zero in the phases with uniform density distribution.

## B. Numerical methods

The starting point of our cluster mean field, hereafter, referred to as cluster Gutzwiller mean-field (CGMF) theory, is to choose an appropriate initial guess state  $|\Psi_{\text{GW}}\rangle$ . From this, we compute the initial  $\phi_{p,q,r}$  and  $n_{p,q,r}$ . In general, we choose the same initial guess state  $|\Psi_\alpha^C\rangle$  for all the  $W$  clusters and consider  $c_{n_0 n_1 \dots n_{m'}}^{(\alpha)} = 1/\sqrt{2^{m'+1}}$ . Then, using corresponding  $\phi_{p,q,r}$  and  $n_{p,q,r}$ , we calculate the Hamiltonian matrix of a cluster given in Eq. (8), which we diagonalize [18,19,84]. We update the state  $|\Psi_{\text{GW}}\rangle$  using the new ground state of the cluster obtained from the diagonalization. Afterwards, we compute  $\phi_{p,q,r}$  and  $n_{p,q,r}$  using this updated  $|\Psi_{\text{GW}}\rangle$ , and advance to the next cluster to repeat the same steps. We sweep the entire lattice system by continuing the procedure, and one such sweep constitutes an iteration. We continue the iterations until desired convergence of  $10^{-12}$  in the  $\phi_{p,q,r}$  and  $n_{p,q,r}$  is obtained. The convergence parameter of quantity is defined as the difference between the values in the present and previous iterations. In our computations, we consider clusters ranging in size from  $1 \times 1 \times 2$  to  $2 \times 2 \times 2$  to tile lattice systems ranging in size from  $8 \times 8 \times 2$  to  $16 \times 16 \times 2$ . To model an uniform infinite lattice system, we employ periodic boundary conditions in  $\phi_{p,q,r}$  and  $n_{p,q,r}$  along  $x$  and  $y$ -directions. We also corroborate the stability of the obtained ground states with respect to different initial guess states having inhomogeneous distribution in  $n_{p,q,r}$  and  $\phi_{p,q,r}$ . The initial guess states considered have checkerboard and random density patterns. For faster computation, we compute the numerical phase boundaries using the bisection method. To identify a phase boundary separating an incompressible and compressible phase, we implement bisection with the SF order parameter  $\phi$  [69]. For a particular  $\mu/V$ , the location of the phase boundary is bracketed within an interval by choosing two values of  $J/V$ . One value lies in the incompressible phase domain and the other in the compressible phase. At each bisection step the interval is halved and the interval which brackets the phase boundary is chosen as the current one. Thus, with  $n$  bisection steps we can determine the phase boundary with an accuracy of  $1/2^n$ . In the present work we use  $n = 14$  and this translates to the accuracy of the phase boundary  $J_c/V$  as  $\approx 6 \times 10^{-5} J/V$ . To further optimize the computation, we limit the number of iterations of the mean-field equation to a few and identify the phase based on the trend of the SF order parameter  $\phi$  from an initial guess value. For a chosen initial value of  $\phi$ , it tends to decrease in the incompressible domain during iteration. Whereas it increases in the compressible domain. These considerations make the computation of phase boundary efficient and allows us to select small step size of  $\delta\mu = 0.02V$ . Thus, the accuracy in the determination of  $J_c/V$  and small  $\delta\mu$  translates to smooth phase boundaries in the phase diagrams. The phase boundary between the structured supersolid and the uniform superfluid phase is obtained similarly by the bisection for the structure factor  $S_r(\pi, \pi)$ .

## C. Quantum phases

The system admits particle and hole vacuum states. And, these states correspond to  $\rho = 0$  and  $\rho = 1$ , respectively. Using the dimer notation these states can be

represented as

$$|\Psi\rangle_{\text{VAC}}^{\rho=0} = \prod_{(p,q)} |00\rangle_{p,q}, \quad (15)$$

and

$$|\Psi\rangle_{\text{VAC}}^{\rho=1} = \prod_{(p,q)} |11\rangle_{p,q}. \quad (16)$$

Thus, in these states, the system either has no atoms or has uniform distribution of one atom per lattice site throughout the system, respectively. The interlayer attractive NN interaction energetically favors the dimer state  $|11\rangle_{p,q}$ . In addition, the intralayer repulsive NN interaction can induce checkerboard density order. This interaction induced spatially periodic intralayer density modulation may be considered as two interpenetrating sublattices, *A* and *B*. It is important to note that  $n_{p,q,1}$  and  $n_{p,q,2}$  have identical distributions or the checkerboard structure in both the layers are aligned. This is due to the attractive interlayer NN interaction, and is in contrast to the case when  $V'$  is repulsive. As mentioned earlier, the Hamiltonian of this system with  $J' = 0$  is equivalent to the two species lattice Hamiltonian in 2D. In which case,  $V'$  is identified as the onsite interspecies interaction strength. For this two-species system with repulsive onsite interspecies interaction the checkerboard structure can have phases with spatially separated density or phase-separated [72].

Due to the intralayer repulsive NN interaction, the bilayer system can exhibit a state of the dimers with solid or diagonal order, which is referred to as dimer checkerboard solid (DCBS). Then, considering the sublattice description of the checkerboard order, the DCBS state can be expressed as

$$|\Psi\rangle_{\text{DCBS}}^{\rho=1/2} = \prod_{(p,q) \in A} |11\rangle_{p,q} \prod_{(p',q') \in B} |00\rangle_{p',q'}. \quad (17)$$

On the other hand, the interlayer hopping can stabilize the triplet state as in Eq. (6). As discussed before, this state with the checkerboard ordered density is the VCBS state. Depending on the average occupancy the VCBS states have the forms

$$|\Psi\rangle_{\text{VCBS}}^{\rho=1/4} = \prod_{(p,q) \in A} |t_0\rangle_{p,q} \prod_{(p',q') \in B} |00\rangle_{p',q'}, \quad (18)$$

and

$$|\Psi\rangle_{\text{VCBS}}^{\rho=3/4} = \prod_{(p,q) \in A} |t_0\rangle_{p,q} \prod_{(p',q') \in B} |11\rangle_{p',q'}. \quad (19)$$

It is important to note that the states described in Eqs. (15)–(19) correspond to the incompressible phases of the bilayer system and the SF order parameter  $\phi_{p,q,r}$  is zero in these phases. In addition, the checkerboard order in the DCBS and VCBS states are quantified by the nonvanishing  $S_r(\pi, \pi)$ . As mentioned earlier, the VCBS states can be distinguished from the DCBS state using the pair and site occupancies,  $\tilde{\rho}_{p,q}$  and  $n_{p,q,r}$ . In the DCBS phase,  $\tilde{\rho}_{p,q}$  and  $n_{p,q,r}$  are finite in the sublattice A, which is evident from Eq. (17). Whereas, in the VCBS phases  $\tilde{\rho}_{p,q}$  is zero but  $n_{p,q,r}$  is finite in the sublattice A. The system also exhibits supersolid and superfluid phases in which  $\phi_{p,q,r}$  is finite. In the SF phase the system has uniform  $n_{p,q,r}$  and  $\phi_{p,q,r}$ . In contrast, the supersolid phase has

checkerboard order in  $n_{p,q,r}$  and  $\phi_{p,q,r}$ . We show the schematic representation of the quantum phases discussed here, in Fig. 2. In the figure, the dimer in the DCBS phase is recognizable, and the blue shade over the bonds indicate the resonating structure of the VCBS states.

Like in the triplet state in the bilayer system, the dipolar atoms in a trilayer optical lattice can exhibit states of the form

$$|w_0\rangle_{p,q} = \frac{1}{\sqrt{3}}(|100\rangle_{p,q} + |010\rangle_{p,q} + |001\rangle_{p,q}), \quad (20)$$

and

$$|w_1\rangle_{p,q} = \frac{1}{\sqrt{3}}(|011\rangle_{p,q} + |101\rangle_{p,q} + |110\rangle_{p,q}). \quad (21)$$

These states have a resonating structure in one of the two sublattices, and are analogous to the VCBS states, given in Eqs. (18) and (19), for a bilayer optical lattice. They are stabilized by the interlayer hopping. They resemble the *W state* of the three qubits that is studied in the context of the quantum information theory [86]. The density of these states can vary as  $\rho = 1/6, 2/6, 4/6$ , and  $5/6$  based on the filling in sublattices A and B. For the  $|w_0\rangle$  state in sublattice A, the density of these states can be  $\rho = 1/6$  and  $4/6$  for the zero and unit filling in sublattice B, respectively. In a similar way, for the  $|w_1\rangle$  state in sublattice A, the density can be  $\rho = 2/6$  and  $5/6$ . On the other hand, the state corresponding to the density  $\rho = 3/6 = 1/2$  does not have a resonating structure unlike others, and is referred to as the trimer checkerboard solid (TCBS) state. The form of this state, in terms of the sublattice description, is

$$|\Psi\rangle_{\text{TCBS}}^{\rho=1/2} = \prod_{(p,q) \in A} |111\rangle_{p,q} \prod_{(p',q') \in B} |000\rangle_{p',q'}. \quad (22)$$

This is a generalization of the DCBS  $\rho = 1/2$  state, given in Eq. (17), for a bilayer optical lattice. It has a checkerboard pattern between sublattices A and B, aligned between the three layers. The same occupancy between the three layers at a given lattice site is the result of the strong attractive interlayer interaction.

#### D. Mean-field phase boundaries

We calculate phase boundaries between the incompressible and compressible phases of the bilayer system using the mean-field theory. We do this by adapting the site-decoupling scheme, and perform perturbative analysis of the mean-field Hamiltonian. In this method, we decompose the creation, annihilation and occupation number operators of a lattice site in terms of the local mean-field and fluctuation operators as  $\hat{b}_{p,q,r} = \phi_{p,q,r} + \delta\hat{b}_{p,q,r}$ ,  $\hat{b}_{p,q,r}^\dagger = \phi_{p,q,r}^* + \delta\hat{b}_{p,q,r}^\dagger$ , and  $\hat{n}_{p,q,r} = n_{p,q,r} + \delta\hat{n}_{p,q,r}$ . Then, the bilinear terms of the Hamiltonian in Eq. (2) are sum of linear terms of the local operators. In the perturbation analysis, we consider the interaction terms as the unperturbed Hamiltonian. These are diagonal with respect to the single site Fock basis states. The off diagonal hopping terms are considered as perturbations. The incompressible to compressible phase boundaries are, then, marked by the vanishing superfluid order parameter, that is  $\phi_{p,q,r} \rightarrow 0^+$ . The  $\phi_{p,q,r}$  being small and associated with the off diagonal terms, it can be considered as the perturbation parameter.

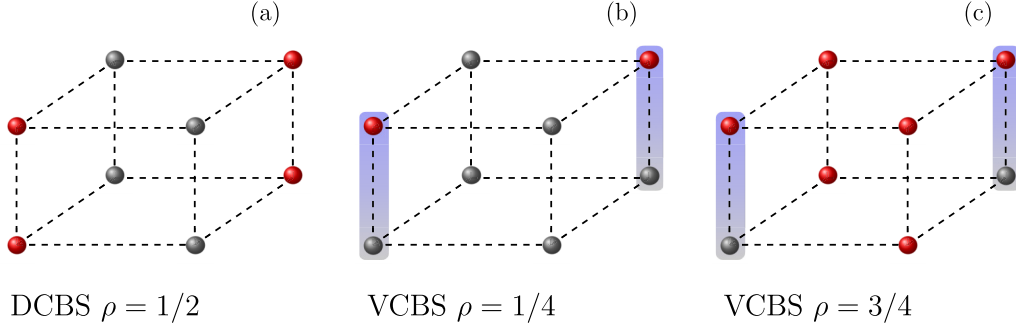


FIG. 2. Schematic representation of the incompressible phases. The red (gray) spheres represent particles or atoms (holes). (a), (b), and (c) correspond to the DCBS, VCBS  $\rho = 1/4$  and VCBS  $\rho = 3/4$  phases, respectively. The blue shading across the interlayer bonds in (b) and (c) denote the entangled state, as given by Eq. (6).

To perform the first-order perturbation analysis, we write the site-decoupled unperturbed Hamiltonian as

$$\begin{aligned} \hat{H}^{(0)} &= \sum_{p,q,r} \hat{h}_{p,q,r}^{(0)} \\ &= \sum_{p,q,r} \hat{n}_{p,q,r} (V' n_{p,q,3-r} + V \bar{n}_{p,q,r} - \mu), \end{aligned} \quad (23)$$

where  $\bar{n}_{p,q,r} = (n_{p+1,q,r} + n_{p-1,q,r} + n_{p,q+1,r} + n_{p,q-1,r})$ , with  $n_{p,q,r} = \langle \hat{n}_{p,q,r} \rangle$  representing the ground state occupancy at the site  $(p, q, r)$ . Now, consider the sublattice description of incompressible states with aligned checkerboard order, the unperturbed energy of the two different sublattices are

$$E_{n_1^A n_2^A}^A = V' n_1^A n_2^A + \sum_{r=1}^2 (4V n_r^A n_r^B - \mu n_r^A), \quad (24)$$

for  $(p, q) \in A$ , and

$$E_{n_1^B n_2^B}^B = V' n_1^B n_2^B + \sum_{r=1}^2 (4V n_r^B n_r^A - \mu n_r^B), \quad (25)$$

for  $(p, q) \in B$ . Here,  $n_r^A$  and  $n_r^B$  are the occupancies in the  $r$ th layer. It is important to note that  $E_{00}^A = E_{00}^B = 0$ . As mentioned earlier, the hopping terms in the Hamiltonian are treated as the perturbations. Then, the site-decoupled perturbation Hamiltonians are

$$\begin{aligned} \hat{T}^A &= -4J \sum_{r=1}^2 \phi_r^B (\hat{b}_r^A + \hat{b}_r^{A\dagger}) - J' \sum_{r=1}^2 \phi_{3-r}^A (\hat{b}_r^A + \hat{b}_r^{A\dagger}), \\ \hat{T}^B &= -4J \sum_{r=1}^2 \phi_r^A (\hat{b}_r^B + \hat{b}_r^{B\dagger}) - J' \sum_{r=1}^2 \phi_{3-r}^B (\hat{b}_r^B + \hat{b}_r^{B\dagger}), \end{aligned}$$

for sublattices  $A$  and  $B$ , respectively. Now, to the first order in the superfluid order parameters, the perturbed ground state is

$$|\chi^\alpha\rangle = |n_1^\alpha n_2^\alpha\rangle + \sum_{\substack{(m_1^\alpha, m_2^\alpha) \\ \neq (n_1^\alpha, n_2^\alpha)}} \frac{\langle m_1^\alpha m_2^\alpha | \hat{T}^\alpha | n_1^\alpha n_2^\alpha \rangle}{(E_{n_1^\alpha n_2^\alpha}^\alpha - E_{m_1^\alpha m_2^\alpha}^\alpha)} |m_1^\alpha m_2^\alpha\rangle, \quad (26)$$

where  $\alpha \in \{A, B\}$ . Then, the superfluid order parameters are  $\phi_k^\alpha = \langle \chi^\alpha | \hat{b}_k^\alpha | \chi^\alpha \rangle$ . In our study, we have considered that the

intralayer parameters are same for both the layers—the layers are identical. Therefore  $\phi_1^A = \phi_2^A = \phi^A$  and  $\phi_1^B = \phi_2^B = \phi^B$ .

We first obtain the phase boundary separating the DCBS phase from a compressible phase, which can either be superfluid or supersolid. The DCBS state in Eq. (17) is an eigenstate of  $\hat{H}^{(0)}$  in Eq. (23), with occupancies  $(n_1^A, n_2^A) = (1, 1)$  and  $(n_1^B, n_2^B) = (0, 0)$ . Then, the superfluid order parameters calculated with respect to the perturbed ground state in Eq. (36) are  $(p, q) \in A$

$$\phi^A = -\frac{4J\phi^B}{(E_{11}^A - E_{01}^A) + J'}, \quad (27)$$

and

$$\phi^B = -\frac{4J\phi^A}{(E_{00}^B - E_{10}^B) + J'}. \quad (28)$$

We solve Eqs. (27) and (28) simultaneously, and then, we take the limit  $\{\phi^A, \phi^B\} \rightarrow 0^+$  to get

$$16J^2 = [(E_{11}^A - E_{01}^A) + J'] \times [(E_{00}^B - E_{10}^B) + J']. \quad (29)$$

Now, substituting the values of  $E_{11}^A, E_{01}^A$  from Eq. (24), and  $E_{10}^B$  from Eq. (25), we obtain the DCBS phase boundary as a solution of

$$16J^2 = (V' - \mu + J')(\mu - 4V + J'). \quad (30)$$

From this, the DCBS lobe in the plane of  $J/V - \mu/V$  can be obtained for different values of  $J'$  and  $V'$ . Similarly, the mean-field phase boundary for the particle and the hole vacuum states given in Eqs. (15) and (16), respectively can be obtained. The phase boundary for the  $|\Psi\rangle_{\text{VAC}}^{\rho=0}$  state is a solution of

$$4J = -\mu - J', \quad (31)$$

while for the  $|\Psi\rangle_{\text{VAC}}^{\rho=1}$  state, it is

$$4J = \mu - 4 - V' - J'. \quad (32)$$

Next, we calculate the equations of the phase boundaries separating the parameter domains of the VCBS states described in Eqs. (18) and (19) from the compressible phases of the system. It is important to notice that these two states are eigenstates of  $\hat{H}^{(0)}$  in Eq. (23). However, as emphasized earlier, the interlayer hopping is essential to stabilize the  $|t_0\rangle_{p,q}$  triplet state of the VCBS states. And, this term is not present in

the site-decoupled unperturbed Hamiltonian  $\hat{H}^{(0)}$ . So, in order to obtain the triplet state  $|t_0\rangle$  as an eigenstate, we define local unperturbed Hamiltonian of sublattice  $A$  as

$$\begin{aligned} \mathcal{H}_A^{(0)} = & -J'(\hat{b}_{p,q,1}^\dagger \hat{b}_{p,q,2} + \text{H.c.}) + V' \hat{n}_{p,q,1} \hat{n}_{p,q,2} \\ & + \sum_{r=1}^2 (V \hat{n}_{p,q,r} \bar{n}_{p,q,r} - \mu \hat{n}_{p,q,r}), \end{aligned} \quad (33)$$

for  $(p, q) \in A$ . Then, we can express the unperturbed ground state energy for sublattice  $A$  as

$$E_{t_0}^A = \langle t_0 | \mathcal{H}_A^{(0)} | t_0 \rangle = -J' + \sum_{r=1}^2 (4V n_r^A n_r^B - \mu n_r^A). \quad (34)$$

This has a contribution from interlayer hopping process, and in contrast to the Eq. (24), it does not have interlayer interaction energy. This is because the pair expectation, as mentioned earlier, is zero with respect to  $|t_0\rangle$ . It is to be noted that in Eq. (34),  $n_1^A = n_2^A = 0.5$ , which are the occupancies calculated with respect to the  $|t_0\rangle$  state. On the other hand, unlike in the previous case, the perturbation Hamiltonian now contains only the intralayer hopping terms, that is,

$$\hat{T}^A = -4J \sum_{r=1}^2 \phi_r^B (\hat{b}_r^A + \hat{b}_r^{A\dagger}). \quad (35)$$

Then, the perturbed ground state is

$$|\chi_{t_0}^A\rangle = |t_0\rangle + \sum_{m_1^A, m_2^A} \frac{\langle m_1^A m_2^A | \hat{T}^A | t_0 \rangle}{(E_{t_0}^A - E_{m_1^A m_2^A}^A)} |m_1^A m_2^A\rangle, \quad (36)$$

where  $(m_1^A, m_2^A) \in \{(0, 0), (1, 1)\}$ . Using this state the superfluid order parameters in sublattice  $A$  can be calculated as  $\phi_r^A = \langle \chi_{t_0}^A | \hat{b}_r^A | \chi_{t_0}^A \rangle$ . Similar to the previous case  $\phi_1^A = \phi_2^A = \varphi^A$ . Then, the superfluid order parameter is

$$\varphi^A = -4J \phi^B \left[ \frac{1}{(E_{t_0}^A - E_{00}^A)} + \frac{1}{(E_{t_0}^A - E_{11}^A)} \right]. \quad (37)$$

For the VCBS state with  $\rho = 1/4$ , we calculate the superfluid order parameter as given in Eq. (37) from the perturbative correction to  $|t_0\rangle_{p,q}$  in sublattice  $A$ . However, we perform the perturbation analysis of the site-decoupled Hamiltonian in sublattice  $B$ . So, we obtain the superfluid order parameter as given in Eq. (28) from the perturbative correction to  $|00\rangle_{p,q}$  state in sublattice  $B$ . We solve the Eqs. (37) and (28) simultaneously, and then take the limit  $\{\varphi^A, \varphi^B\} \rightarrow 0^+$  to obtain

$$\begin{aligned} \frac{1}{16J^2} = & \left[ \frac{1}{(E_{t_0}^A - E_{00}^A)} + \frac{1}{(E_{t_0}^A - E_{11}^A)} \right] \\ & \times \left[ \frac{1}{(E_{00}^B - E_{10}^B) + J'} \right]. \end{aligned} \quad (38)$$

Note that, for the unperturbed ground state the occupancies  $(n_1^A, n_2^A) = (0.5, 0.5)$  and  $(n_1^B, n_2^B) = (0, 0)$ . Now, by substituting the values of  $E_{t_0}^A$  from Eq. (34),  $E_{11}^A$  from Eq. (34), and  $E_{10}^B$  from Eq. (34), we obtain the VCBS ( $\rho = 1/4$ ) phase

boundary as a solution of

$$16J^2(2J' + V') = (\mu - 2V + J')(J' + \mu)(\mu - J' - V'). \quad (39)$$

It is worth mentioning that  $E_{11}^A$  from Eq. (34) is equal to  $\langle 11 | \mathcal{H}_A^{(0)} | 11 \rangle$ . Similarly, for the VCBS state with  $\rho = 3/4$ , we perform the perturbative analysis to state  $|11\rangle_{p,q}$  in sublattice  $B$ . We obtain the expression of the superfluid order parameter  $\varphi^B$ , which is similar to the Eq. (28) with the superscripts  $A$  and  $B$  interchanged. We, then simultaneously solve this equation and Eq. (37), and take the limit  $\{\varphi^A, \varphi^B\} \rightarrow 0^+$  like in the previous case. Then, we obtain the VCBS ( $\rho = 3/4$ ) phase boundary as a solution of

$$\begin{aligned} 16J^2(2J' + V') = & (2V + V' - \mu + J')(\mu - 4V + J') \\ & \times (\mu - J' - 4V - V'). \end{aligned} \quad (40)$$

From Eqs. (39) and (40), the VCBS lobes with  $\rho = 1/4$  and  $3/4$  can be obtained in the  $J/V - \mu/V$  plane for different values of  $J'$  and  $V'$ .

The above formalism can be generalized to the trilayer system and the details of the derivation are given in the Appendix B. The equation defining the phase boundary between the TCBS phase and the compressible phase is

$$16J^2 = (2V' - \mu + 2J')(\mu - 4V + 2J'). \quad (41)$$

Based on this, the VCBS ( $\rho = 1/6$ ) phase to compressible phase boundary is given by

$$16J^2(3V' + \mu + 8J') = (3\mu - 4V + 6J')(\mu + 2J')(\mu - V'), \quad (42)$$

and that of VCBS ( $\rho = 2/6$ ) is

$$\begin{aligned} 16J^2(5V' - \mu + 8J') = & (3\mu - 8V + 6J') \\ & \times (\mu - 2V' - 2J')(\mu - V'). \end{aligned} \quad (43)$$

Invoking the particle-hole symmetry of the model, we can write the phase boundaries between the VCBS  $\rho = 4/6$  and the compressible phase as

$$\begin{aligned} 16J^2(3V' - 4V + \mu + 8J') = & (6J' + 4V + 6V' - 3\mu) \\ & \times (4V - \mu - 2J')(-\mu + V' + 4V), \end{aligned} \quad (44)$$

and that of VCBS  $\rho = 5/6$  as

$$\begin{aligned} 16J^2(5V' + 4V - \mu + 8J') = & (6J' + 8V + 6V' - 3\mu) \\ & \times (4V - \mu + 2J' + 2V')(-\mu + V' + 4V). \end{aligned} \quad (45)$$

The phase diagram obtained based on these equations, shown in the results section, is in good agreement with the one obtained numerically.

#### IV. RESULTS AND DISCUSSIONS

To find the ground state of the bilayer system, we first scale the Hamiltonian in Eq. (2) by the intralayer NN interaction strength  $V$ . This choice yields four independent parameters,  $J/V$ ,  $J'/V$ ,  $V'/V$  and  $\mu/V$ , which can be varied to probe different quantum phases of the system. We present the parameter domains of these quantum phases in the  $J/V - \mu/V$  plane for fixed values of  $V'/V$  and  $J'/V$ . To begin with we

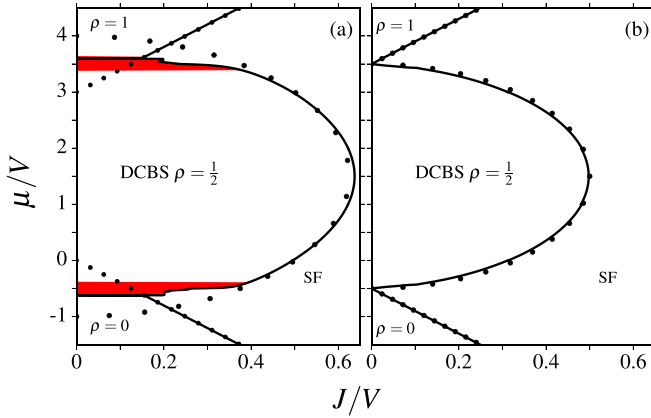


FIG. 3. Phase diagrams in the  $J/V - \mu/V$  plane for  $J'/V = 0$  and  $0.5$ , respectively for  $V' = -1.0V$ . The black lines represent the phase boundaries between the incompressible and compressible phases, obtained numerically with  $2 \times 2 \times 2$  clusters in the CGMF method. Metastable quantum phases with intermediate values of  $\rho$  are present in the red shaded region in the phase diagram. And, the filled black circles denote the analytical phase boundaries obtained from the site-decoupled mean-field method, as given in Eqs. (30)–(32).

consider the case when  $V'/V = -1$ , and examine the quantum phases in three broad domains of interlayer hopping. These are weak ( $J'/V = 0$  and  $0.5$ ), moderate ( $J'/V = 0.8$  and  $1.0$ ), and strong ( $J'/V = 1.2$  and  $1.5$ ) interlayer hopping. We present and discuss the corresponding phase diagrams in Sec. IV A. Then, we also examine the effects of the quantum correlations on the parameter domains of the quantum phases. We then consider the case of  $|V'| \neq V$  in Sec. IV B. As representative cases we consider  $V' = -0.25V$  and  $-2.0V$ . The effect of the thermal fluctuations is discussed in Sec. IV C. Considering the influence of thermal fluctuations on the quantum phases is essential to relate our results to the possible experimental realizations.

#### A. $V' = -1.0V$

This is a suitable choice to probe the interplay between different hopping and interaction energies theoretically. In terms of lattice constants, it corresponds to  $a_z = \sqrt[3]{2}a$ . We extend the theoretical insights gained from this case to the  $|V'| \neq V$  regime.

##### 1. Weak interlayer hopping $J'/V < 1$

In this domain, we consider two values of  $J'/V = 0, 0.5$ . The corresponding phase diagrams are shown in Figs. 3(a) and 3(b), respectively. For  $J'/V = 0$ , the interlayer hopping is absent, and the two layers are coupled only through the NN attractive interaction. As mentioned earlier, this is equivalent to the two-species extended Bose-Hubbard model for hardcore bosons with attractive onsite and zero offsite interspecies interaction strengths [72]. In Fig. 3, the solid lines represent the phase boundaries obtained numerically with  $2 \times 2 \times 2$  clusters in the CGMF method. Here after, for compact notation, we shall refer to the  $2 \times 2 \times 2$  cluster as the  $2^3$  cluster. The filled circles mark the incompressible-

compressible phase boundaries obtained analytically from the site-decoupled mean-field theory. In particular, the filled circles in Figs. 3(a) and 3(b) represent the phase boundary of the DCBS phase obtained by solving the Eq. (30) with  $V' = -1.0V$ ,  $J' = 0V$  and  $0.5V$ , respectively. It is evident from the Fig. 3(a) that the numerical and analytical results are in good agreement for  $J/V \geq 0.34$ . In this parameter regime the difference between the numerical and analytical results are below  $0.1\mu/V$ . It is, however, larger for  $J/V < 0.34$ . This is due to merging of the incompressible lobes and the applicability of site-decoupled mean field to discern only incompressible-compressible phase boundaries. The merger of the DCBS  $\rho = 1/2$  and uniform  $\rho = 0, 1$  state lobes result in the emergence of incompressible states with intermediate values of  $\rho$ . In our computations, these states are dependent on the initial conditions, and vary with the values of  $\mu/V$  and  $J/V$ , indicating metastability for these parameter domains. This may signify a first-order phase transition between the incompressible states or the presence of emulsion phases [16,17]. In Fig. 3(a), the shaded regions indicate the parameter domains of these states. Similar feature was also reported in the previous studies with attractive interactions [16,17,87]. It is to be noted that in these regions, an incompressible ground state required for the perturbative analysis is ill defined. In contrast, for our perturbative analysis either the uniform  $\rho = 0, 1$  or DCBS  $\rho = 1/2$  state is taken as the reference state to calculate the incompressible-compressible phase boundaries. This is the reason for the poor agreement between the analytical and numerical phase boundaries in Fig. 3(a). The overlapping analytical phase boundaries of the incompressible phases indicate the merging of the incompressible lobes. However, the numerically obtained states have lower energy than the considered incompressible states in the perturbative analysis. So, in the suppressed interlayer and the weak intralayer hopping regime, the numerical phase-boundaries provide better description of the parameter domains of quantum phases. The merger of the incompressible lobes is a result of the attractive interlayer interaction but suppressed interlayer hopping. More importantly, the merging of the parameter domains leads to emergence of triple points [17] at  $\mu/V = 3.57$  and  $\mu/V = -0.57$  for  $J/V = 0.138$  in Fig. 3(a). With the increase in the  $J'/V$  the triple points shift towards left due to enhanced kinetic energy of the system. And, the points reside on the  $\mu/V = 0$  axis for  $J'/V \gtrsim 0.3$ .

From Fig. 3(a), it is evident that the ground state is either MI with  $\rho = 0$  and  $\rho = 1$ , or a DCBS state with  $\rho = 1/2$ . The DCBS state has checkerboard order of the dimers, and can be described as in Eq. (17). The checkerboard ordering is due to the intralayer NN repulsive interaction, which disfavors phases with density like the MI phase. It is important to note that MI phases sandwich the DCBS phase. This is because, the DCBS state can be obtained through dimer creation and annihilation from the MI  $\rho = 0$  and  $\rho = 1$  states, respectively. This feature of the DCBS state is also evident from the comparison between the Eqs. (15)–(17). At higher  $J/V$ , the atoms in the lattice acquire enough kinetic energy, and they become itinerant. So, the system exhibit SF phase with uniform density distribution. In this phase  $\phi_{p,q,r}$  is finite and uniform throughout the lattice.

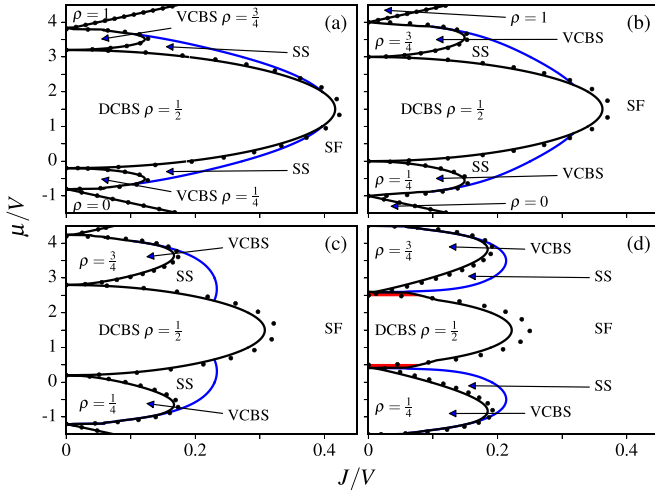


FIG. 4. Phase diagrams in the  $J'/V - \mu/V$  plane for  $J'/V = 0.8, 1.0, 1.2$  and  $1.5$  for  $V'/V = -1.0$  are shown in (a), (b), (c), and (d), respectively. The black lines indicate the phase boundaries between the incompressible and compressible phases, and the blue lines represent the SS-to-SF phase boundary, which are computed numerically with  $2 \times 2 \times 2$  clusters in the CGMF method. Filled black circles are the phase boundaries obtained from the perturbative analysis of the mean-field Hamiltonian, as given in the Eqs. (30), (31), (32), (39), and (40). The red shaded region in the (d) corresponds to an incompressible phase with no dimer structure.

For  $J'/V = 0.5$ , the qualitative features of the phase diagram are similar to  $J'/V = 0$ . However, the nonzero value of the interlayer hopping disfavors the dimer state, and the DCBS  $\rho = 1/2$  lobe shrinks. This can be observed from a comparison between Figs. 3(a) and 3(b). The interlayer hopping is, however, not sufficiently strong to favor the triplet state as in Eq. (6). The shrinking of incompressible lobes like the DCBS at higher hopping strength is a common feature of optical lattice system. The system tends to exhibit compressible phases as the total hopping energy is enhanced. So, the DCBS lobe continues to shrink with further increase in  $J'/V$ , which can also be read off from Fig. 4.

## 2. Moderate interlayer hopping $J'/V \approx 1$

We consider  $J'/V = 0.8$  and  $1$  as representative cases for this domain, and the phase diagrams are shown in Figs. 4(a) and 4(b), respectively. As in the previous case, the solid black lines are the numerical phase boundaries. And, the filled circles are the analytical solutions of Eqs. (30), (39), and (40) for the DCBS  $\rho = 1/2$ , VCBS  $\rho = 1/4$ , and VCBS  $3/4$  states, respectively. One striking feature of the phase diagrams is the presence of the VCBS phase. In these states, the occupancy can be thought as resonating between two NN lattice sites in different layers, which corresponds to the triplet state in Eq. (6). This triplet state is stabilized by the interlayer hopping, and the VCBS states appear when  $J'/V > 0.5$ . They emerge as small lobes above and below the DCBS lobe, and grows with the increase in  $J'/V$ . This is because, the  $\rho = 1/4$  and  $3/4$  VCBS states are the hole and particle excitations of the DCBS  $\rho = 1/2$  state, respectively. This is also evident from the comparison of the Eqs. (17)–(19). Thus, besides the

MI and DCBS states, the system hosts the VCBS states at low values of  $J'/V$ . In addition, the compressible SS phases also appears in between the DCBS and VCBS phases. In the SS phase, both the diagonal and off-diagonal long-range order are present. That is, it has the superfluid characteristics and the periodic modulation in  $n_{p,q,r}$  distribution. These are characterized by the finite values of  $\phi_{p,q,r}$  and  $S_r(\pi, \pi)$ , respectively. For larger values of  $J'/V$ , the system is in the SF phase with uniform  $n_{p,q,r}$  and  $\phi_{p,q,r}$ .

Comparing Figs. 4(a) and 4(b), we observe an enhancement in the domains of the VCBS and SS phases. This implies that the VCBS phase, even though incompressible, is stabilized by the large interlayer hopping. This needs to be contrasted with the DCBS phase, for which the domain shrinks with increased hopping strength. The enhancement of the SS domain indicates that the SS phase originates from the intralayer hopping induced particle-hole excitations to the VCBS states, but not to the DCBS state. This is corroborated later by considering stronger interlayer hopping strength. We also observe good agreement between the analytical and numerical phase boundaries of the VCBS states. Whereas, for the DCBS phase, the analytical results tend to over estimate the phase boundary. This is because, the VCBS states are eigenstates of the unperturbed Hamiltonian in Eq. (33), which has the interlayer hopping term. So, as in the CGMF method, the interlayer hopping term is treated exactly in the analytical approach. However, for the DCBS state, the site-decoupled mean-field analysis is applicable. It treats all the intra- and interlayer hopping as perturbations and fails to capture the domain with large hopping.

## 3. Strong interlayer hopping $J'/V > 1.0$

We consider  $J'/V = 1.2$  and  $1.5$  as representative cases of this domain. And, the phase diagrams are shown in Figs. 4(c) and 4(d), respectively. The VCBS states are more prominent with higher  $J'/V$ . The DCBS  $\rho = 1/2$ , on the other hand, continues to shrink with the increase in  $J'/V$ . And, this is consistent with the earlier observation. For  $J'/V = 1.5$ , the extent of the DCBS and VCBS lobes are comparable. It is important to note that the SS phases are sandwiched between the VCBS and DCBS lobes. However, the extent of these domains around the DCBS lobe shrink with the increase in  $J'/V$ . That is, the domains detach from the DCBS lobe. And, the SS phase surround only the VCBS lobes when  $J'/V = 1.5$ . This implies that the SS phase in our study is created through the particle-hole excitations to the VCBS states. Hence, this state may be referred to as the valence bond SS (VSS) state.

An emergent feature of the strong interlayer hopping is the quantum phase in the shaded parameter domain in the phase diagram. This occurs for  $\mu/V \in [0.4, 0.5]$  and  $\mu/V \in [2.5, 2.6]$ , in the phase diagram as shown in the Fig. 4(d). The discernible distortion of the phase boundary in this region is due to a new incompressible phase which replaces the DCBS phase. The intralayer and interlayer density distributions exhibit checkerboard order with a two sublattice structure, and average density is  $\rho = 0.5$ . The occupancies, however, are real for both the layers. Unlike the DCBS phase, the pair expectation between the two layers of this phase is  $\approx 10^{-4}$ , which highlights the nondimer structure. The stability of this

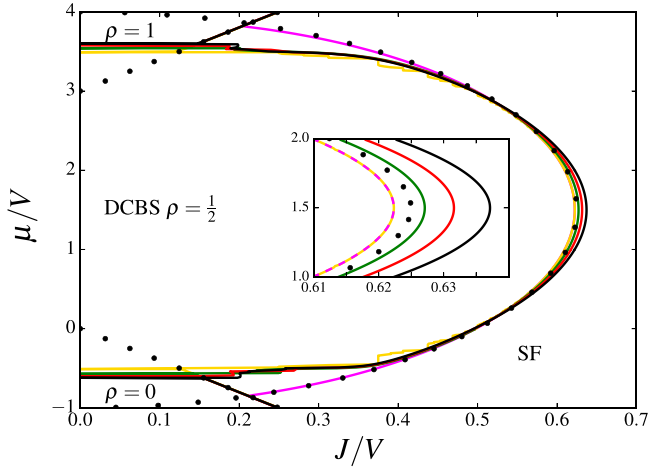


FIG. 5. Phase diagrams of the bilayer optical lattice in the  $J/V - \mu/V$  plane for  $J'/V = 0$  and  $V'/V = -1.0$  obtained from the clusters of different sizes:  $1 \times 1 \times 1$  (magenta),  $1 \times 1 \times 2$  (gold),  $2 \times 1 \times 2$  (green),  $4 \times 1 \times 2$  (red), and  $2 \times 2 \times 2$  (black). The filled black circles represent the analytically obtained phase boundary obtained from the Eqs. (30)–(32).

phase is the strong interlayer hopping, which prefers the basis states allowing maximal interlayer hopping. For  $\mu/V = 0.5$  to  $0.6$ , this new phase is metastable and competes with the energetically lower DCBS phase. Further studies, in the strong interlayer hopping domain are underway, to understand the properties of the quantum phases in this domain.

An important feature of all the phase diagrams in Figs. 3 and 4 is the vertical symmetry of the quantum phases around the  $\mu/V = 1.5$  axis. This is due to the underlying particle-hole symmetry of the system Hamiltonian. From the Eq. (A4), it is evident that the particle-hole symmetry point is at  $\mu/V = 1.5$  for  $V' = -1.0V$ ,

#### 4. Quantum fluctuations

The phase diagrams considered so far are computed with the  $2^3$  clusters. To understand the effects of the quantum fluctuations to the quantum phases, we perform computations by varying the cluster sizes from a single site to  $4 \times 1 \times 2$ . In the CGMF method, quantum correlations are better described with increasing cluster size. Thus the method provides better results with larger clusters.

We first consider the case of  $J'/V = 0$ , to analyze quantitative changes of the DCBS  $\rho = 1/2$  lobe with different cluster sizes. The phase diagram is shown in Fig. 5. The phase boundary near the tip of the lobe shows marginal enlargement with the increase in cluster size. For comparison we mark the analytically determined phase boundary by black filled circles. This, except for minor deviations around the tip of the DCBS lobe, is in good agreement with the single-site numerical results. The agreement is an expected feature as the site-decoupled mean-field theory is equivalent to single-site mean-field theory in determining the incompressible-compressible phase boundaries. The deviation around the tip can be attributed to the large value of  $J/V$  and the numerical threshold in the value of the superfluid order parameter. Another interesting aspect of the figure is

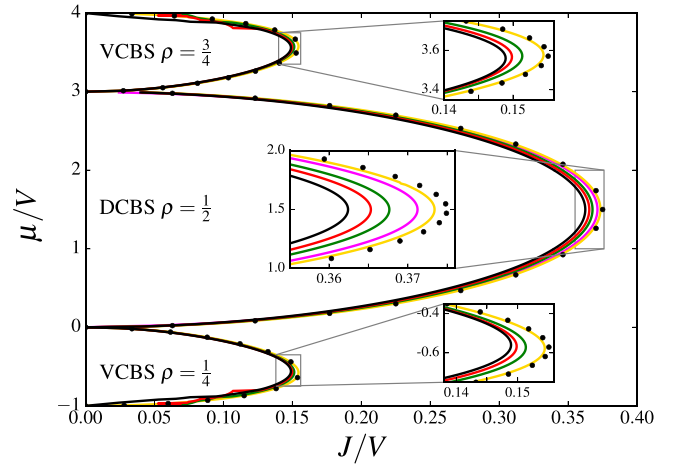


FIG. 6. The incompressible to compressible phase boundaries in the  $J/V - \mu/V$  plane for  $J'/V = 1.0$  and  $V'/V = -1.0$  obtained from clusters of different sizes:  $1 \times 1 \times 1$  (magenta),  $1 \times 1 \times 2$  (gold), green for  $2 \times 1 \times 2$  (green),  $4 \times 1 \times 2$  (red), and  $2 \times 2 \times 2$  (black). The filled black circles indicate the analytical phase boundaries obtained from Eqs. (30), (39), and (40).

the overlap of the phase boundaries obtained from single-site and  $1 \times 1 \times 2$  clusters. This is because, for  $J'/V = 0$  the interlayer coupling is only through interlayer interaction. So, in the intralayer hopping dominated regime, large  $J/V$ , the two are expected to give similar results. In this domain the results, however, improve with the increase in the intralayer cluster size, for example, with  $2 \times 1 \times 2$ ,  $4 \times 1 \times 2$ , and  $2^3$  clusters. On the other hand, the phase boundaries obtained from single-site and  $1 \times 1 \times 2$  clusters do not match in the low  $J/V$  regime. In this domain, the quantum phases are determined by the interaction energy, and is better described by the  $1 \times 1 \times 2$  cluster.

Next, we consider the case of  $J'/V = 1$ , and study the impact of quantum fluctuations on the VCBS  $\rho = 1/4$  and  $3/4$ , and DCBS  $\rho = 1/2$  phases. The VCBS states has checkerboard distribution of the maximally entangled triplet state. So, it is important to study the effects of the quantum correlations, better described by the CGMF method with larger cluster sizes, on the VCBS phase. For this, we obtain phase diagram by varying the cluster size. We observe that the VCBS lobes shrink with the increase in cluster size, shown as insets in Fig. 6. Note that the single-site theory cannot describe the VCBS states due to absence of the minimal intersite correlations required to represent the state. Therefore the phase boundaries of the VCBS states are obtained using  $1 \times 1 \times 2$ ,  $2 \times 1 \times 2$ ,  $4 \times 1 \times 2$ , and  $2^3$  clusters. In addition, we illustrate the analytical phase boundaries obtained by solving Eqs. (39) and (40), which are in agreement with the phase boundaries obtained using  $1 \times 1 \times 2$  cluster. This is because, the unperturbed Hamiltonian in Eq. (33) treats the interlayer hopping term exactly, and the intralayer hopping terms are considered as perturbation with the SF order parameter as perturbation parameter. So, this is similar to the mean-field Hamiltonian considered in the CGMF method for  $1 \times 1 \times 2$  cluster. It is important to note that, unlike the  $J'/V = 0$  case, now the DCBS lobe shrinks with the increase in cluster size.

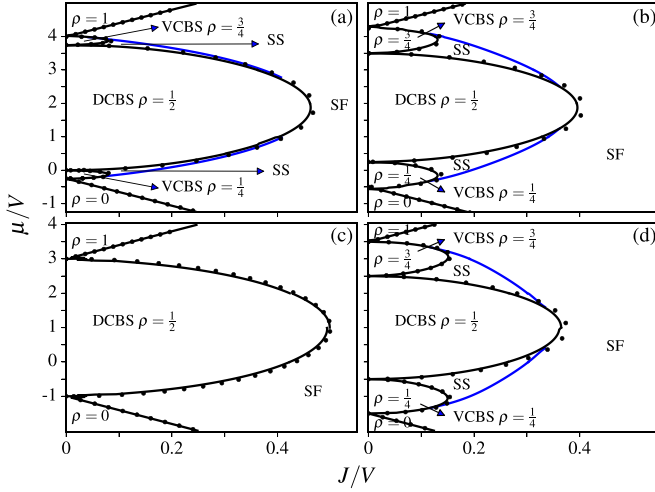


FIG. 7. Phase diagram in the  $J/V$ - $\mu/V$  plane for  $V'/V = -0.25$  (top) and  $V'/V = -2.0$  (bottom). The subplots (a) and (b) correspond to  $J'/V = 0.25$  and  $0.5$ , respectively. The subplots (c) and (d) correspond to  $J'/V = 1.0$  and  $1.5$ , respectively. The black solid lines represent the phase boundaries between incompressible and compressible phases, and the blue lines indicate the phase boundaries between SS and SF phases. These phase boundaries are obtained numerically using  $2 \times 2 \times 2$  clusters in the CGMF method. The black circles represent the analytically obtained phase boundary points obtained from the Eqs. (30), (31), (32), (39), and (40).

This is evident from the phase boundaries shown as inset in Figs. 5 and 6 for the DCBS lobe.

In addition, to verify the robustness of the quantum phases against quantum correlations and fluctuations, we have calculated the ground state with exact-diagonalization with system size  $4 \times 4 \times 2$  at different hopping strengths and values of  $\rho$ . We, however, do not generate the phase diagrams using  $4 \times 4 \times 2$  cluster due to large size of the Hamiltonian matrix as the local Hilbert space grows exponentially with the cluster size. This leads to long computational time to obtain the phase boundaries.

### B. $V' \neq V$ case

The results discussed so far consider identical intralayer repulsive and interlayer attractive NN interactions. Now we consider the regime with asymmetric NN interaction strengths. In particular, we consider the cases of  $V' = -0.25V$  and  $-2V$ . The former is motivated by the experimental study of Baier *et al.* [6]. In the experiment, the wavelengths of the lasers generating the optical lattice have the ratios  $\lambda_x : \lambda_y : \lambda_z = 1 : 1 : 2$ . This implies  $a_z = 2a$  and corresponds to  $V' = -0.25V$ . The case of  $V' = -2V$  corresponds to  $a_z = a(\lambda_x : \lambda_y : \lambda_z = 1 : 1 : 1)$  and the optical lattice has cubic unit cell.

#### 1. $V' = -0.25V$

The phase diagram for  $J'/V = 0.25$  and  $0.50$  are shown in Figs. 7(a) and 7(b), respectively. The phase diagrams are symmetric about the particle-hole symmetry point  $\mu/V = 1.875$ . And, we obtain the same value from the analytic expression in Eq. (A4). In the phase diagram, the VCBS  $\rho = 1/4$  and  $3/4$

lobes are small. This is due to the weak interlayer hopping strength and these lobes emerge when  $J'/V > 0.13$ . Like in  $V' = -V$ , we observe domains of SS phase which originate from the edge of the VCBS lobes, and terminate on the DCBS lobe. On increasing  $J'/V$  to  $0.5$ , the VCBS lobes are enhanced and so do the domains of the SS phase. In contrast the DCBS lobe, liker earlier cases, shrinks in size. For both the values of  $J'/V$ , the phase boundaries obtained analytically are in good agreement with the numerical results.

#### 2. $V' = -2V$

The phase diagrams for this case are shown in Figs. 7(c) and 7(d), and these correspond to the interlayer hopping strengths  $J'/V = 1$  and  $1.5$ , respectively. An important feature of the phase diagram in Fig. 7(c) is the absence of the VCBS phase. The phase diagram is thus qualitatively similar to the phase diagram in Fig. 3(b). This indicates that a larger interlayer hopping  $J'/V$  is essential for the VCBS phase to appear in the system. This ensures that one of the sublattice has triplet state  $|t_0\rangle$  as a ground state, which is a characteristic of the VCBS phase. We observe the VCBS state enters as a possible ground state when  $J'/V > 1$ . So, based on the phase diagrams for  $V'/V = -1, -0.25$ , and  $-2$ , the system may exhibit the VCBS phase when  $J' > |V|/2$ .

### C. Finite-temperature phase diagram

The results discussed so far are obtained at zero temperature. These provide qualitative descriptions of the quantum phases present in the system. This follows from the characterization of quantum phases and quantum phase transitions as zero temperature phenomena. Experimental realizations, however, are at finite temperatures. So, we incorporate the effects of temperature on the quantum phases, and examine the domains in the phase diagrams. The quantum phases are known to “melt” by the thermal fluctuations associated with finite temperatures. Thus, at finite temperature, the system exhibits a normal fluid (NF) phase. It is characterized by zero SF order parameter and real occupancy at each lattice site [18,19,72,88–90]. This is to be contrasted with the incompressible quantum phases, which have integer occupancy at each lattice site and zero SF order parameter.

The finite temperature calculations require thermal averaging of the observables. This is done by computing the partition function of a cluster as

$$Z = \sum_l e^{-\beta E_l}, \quad (46)$$

where  $\beta = 1/k_B T$ ,  $k_B$  is the Boltzmann constant,  $T$  is the temperature of the system, and  $E_l$  is the  $l$ th eigenvalue of the cluster Hamiltonian  $\hat{H}_C$  in Eq. (8). Then, the thermal average of a local operator  $\hat{O}_{p,q}$  at the site  $(p, q)$  within the cluster is

$$\langle\langle \hat{O}_{p,q} \rangle\rangle = \frac{1}{Z} \text{Tr}(e^{-\beta \hat{H}_C} \hat{O}_{p,q}), \quad (47)$$

where  $\langle\langle \dots \rangle\rangle$  denotes thermal average, and here the trace is calculated with respect to the eigenstates of the cluster Hamiltonian. The details of the finite temperature computations with the CGMF method are given in our previous work [18]. Owing to the better representation of the eigen energies

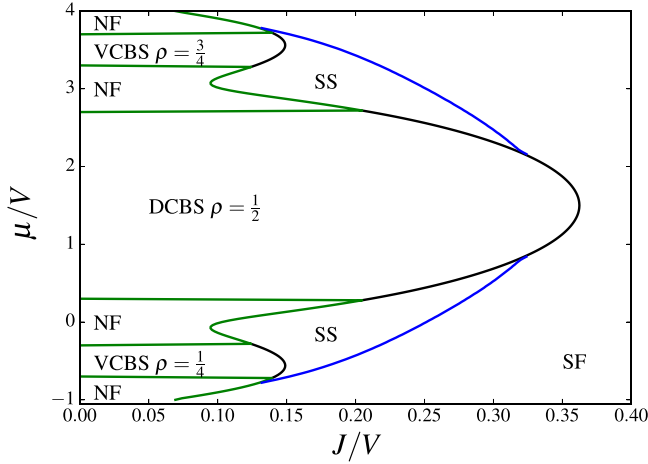


FIG. 8. Finite temperature phase diagram for the bilayer optical lattice in the  $J/V$ - $\mu/V$  plane for  $J'/V = 1.0$ ,  $V'/V = -1.0$ , and  $k_B T = 0.05V$ . The phase boundaries are obtained numerically with  $2 \times 2 \times 2$  clusters in the CGMF method. The green lines represent the phase boundary between the NF and the compressible phase, while black lines indicate the phase boundaries between incompressible, unmelted phases and compressible phases.

and eigenstates of the system with larger size clusters, the thermal fluctuations are better described by the clusters of larger sizes. However, it is to be noted that our study is in the strong on-site interaction regime. In this regime, the intersite coupling is weak and the ground state can be considered as a product state. Thus, the Gutzwiller mean-field ansatz is a good choice and captures the gapped incompressible phases. In our simulations, we have observed that the gap is of the order of temperature considered near the phase boundaries. Thus, the effects of finite temperature on the zero-temperature quantum phases are qualitatively well described by the thermal averaging in Eq. (47). This thermal averaging is incorporated self-consistently for SF order parameters and site occupancies in the cluster Hamiltonian in Eq. (8). Alternatively, the thermal averages of physical quantities can also be computed from the low energy collective excitations obtained through variants of mean-field theory [21–26,72,91]. In the gapless superfluid regime, these techniques describe the effects of the finite temperature. We consider  $J'/V = 1$  and  $V'/V = -1$  as a representative case to examine the effects of thermal fluctuations and phase diagram is shown in Fig. 8 for  $k_B T = 0.05V$ . To estimate the corresponding temperature, we have considered the system parameters from the experimental work of Baier *et al.* [6]. Then, the  $k_B T = 0.05V$  correspond to  $T \approx 0.1$  nK. We observe the melting of the DCBS and VCBS phases at the top and bottom domains of the lobes. These are the parameter domains where the lobes close and density fluctuations are prominent. So, it is natural for the thermal fluctuation effects to be higher in these domains and melting to commence. The phase fluctuations are dominant around the tip of the lobes and the quantum phases persist. A sequence of finite temperatures computations around the tip of the solid DCBS lobes shows that it can persist upto  $T \approx 1.0$  nK. While, for the VCBS lobe, the melting temperature is  $T \approx 0.2$  nK. These are consistent with the estimate of  $T \lesssim 1.5$  nK by Baier and collaborators [6] to observe novel stripe phases in their experiment. As

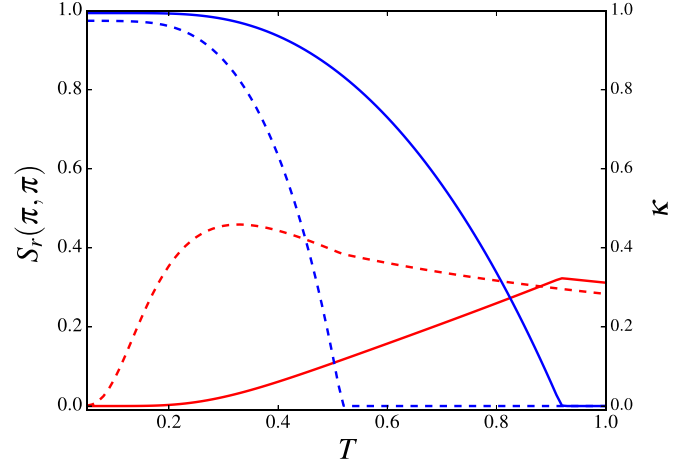


FIG. 9. Plot of the  $\kappa$  and  $S_r(\pi, \pi)$  as a function of temperature. The blue solid (dashed) line indicates the  $S_r(\pi, \pi)$  for DCBS  $\rho = 1/2$  (VCBS  $\rho = 1/4$ ) state at low temperatures. The red solid (dashed) line indicates the  $\kappa$  for DCBS  $\rho = 1/2$  (VCBS  $\rho = 1/4$ ) state. Here the system parameters  $J'/V = 1.0$  and  $V'/V = -1.0$  are considered. The value of  $J/V$  is fixed at 0.08, and the values of the chemical potential  $\mu/V$  are  $-0.5$  and  $1.5$  for VCBS ( $\rho = 1/4$ ) and DCBS phases, respectively.

mentioned earlier,  $\phi$  is zero in the NF phase, but has nonzero number fluctuation. Thus, the NF-SS and NF-SF phase boundaries are obtained by locating  $J_c/V$  at which  $\phi$  becomes nonzero. However, to distinguish the NF phase from the incompressible quantum phases, we consider compressibility  $\kappa$  as the order parameter. The NF phase possesses finite  $\kappa$ , but it is negligibly small for the incompressible quantum phases. For example, it is of  $O(10^{-1})$  within the NF domain, while for the incompressible quantum phases, it is of the  $O(10^{-6})$ . One point to be noted is, at finite temperatures the number fluctuations, however small, are present in all the quantum phases. And this leads to finite  $\kappa$  for all the quantum phases. So, to identify the NF-VCBS or NF-DCBS phase boundary an appropriate threshold value for  $\kappa$  is to be chosen. This is also a characteristic of a continuous phase transition. Earlier works [88,89] have reported the condition on  $\kappa$  to distinguish the NF phase from the incompressible quantum phases. In the present work, we consider the threshold value of  $\kappa$  as  $0.04/V$ . That is,  $\kappa > 0.04/V$  indicates the melting of the quantum phases, and thus, the presence of NF phase.

One important feature of the NF phase is, it inherits the density order of the original incompressible phase. For example, melting of the checkerboard incompressible quantum phases forms a checkerboard NF (CBNF) phase. The checkerboard order vanishes at higher temperature, and we obtain uniform density NF phase. To illustrate the transition, we plot the  $S_r(\pi, \pi)$  and the  $\kappa$  as a function of temperature in Fig. 9. The CBNF domain is identified by the nonzero  $S_r(\pi, \pi)$  and  $\kappa$  and occurs at lower temperatures. With the increase in temperature  $S_r(\pi, \pi)$  decrease and becomes zero at  $T = 0.92$  and  $0.52$  for the DCBS and VCBS  $\rho = 1/4$  phases, respectively. In this domain, the NF phase has uniform density distribution. However, the particle-hole symmetry of the phase diagram is robust against thermal fluctuations and persists at finite temperatures. That is, the melting of the quantum phases is

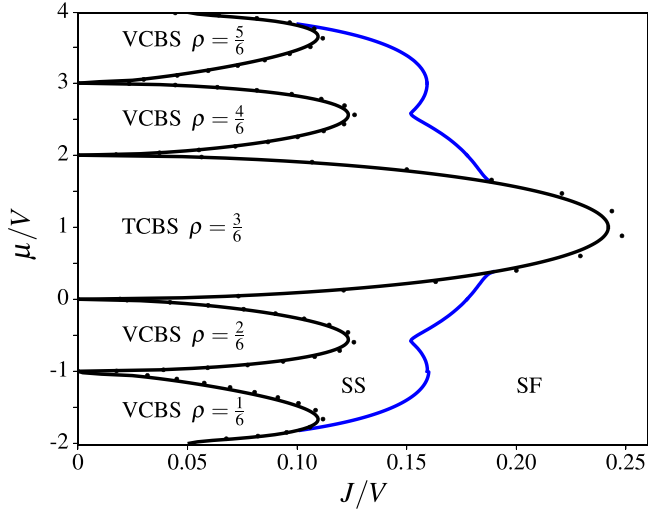


FIG. 10. Phase diagram for trilayer optical lattice in the  $J/V$ - $\mu/V$  plane for  $J'/V = 1$  and  $V'/V = -1$ . The black solid lines represent the phase boundaries between incompressible and compressible phases, and the blue lines indicate the phase boundaries between SS and SF phase, obtained numerically with  $2 \times 1 \times 3$  clusters in the CGMF method and with periodic boundary condition along  $z$  direction. The black circles represent the analytically obtained phase boundary points from the Eqs. (41)–(45).

symmetric about  $\mu/V = 1.5$ . It is important to notice that for a fixed value of  $J/V$ , the VCBS states melt at lower temperatures than the DCBS state. This can be read off from Fig. 9. The melting of the VCBS phase at a lower temperature implies that the VCBS states are entangled and have larger quantum correlation embedded. This renders the phase fragile against the thermal fluctuations.

#### D. Phase diagrams of trilayer system

We now consider introducing an additional layer to the bilayer system and make it a trilayer system. The Hamiltonian of the system is given by the Eq. (5) with  $M = 3$ . We, then, investigate the quantum phases emerging due to the competition between the interlayer hopping and interlayer interaction. For illustration, we consider  $V' = -V$ , and  $J' = V$ , and the phase diagram in the  $J/V - \mu/V$  plane, is shown in Fig. 10.

At low  $J/V$ , the ground state is either the VCBS state, or a trimer checkerboard solid (TCBS) state. The TCBS lobe corresponds to the  $\rho = 1/2$ , and is the central large lobe in the phase diagram. This state is an analog of the DCBS  $\rho = 1/2$  state in the bilayer system, and is incompressible. The two lobes below the TCBS lobe are the VCBS  $\rho = 1/6$  and  $2/6$  lobes, in the increasing order of  $\mu/V$ . And, the two lobes above the TCBS lobe are of the VCBS  $\rho = 4/6$  and VCBS  $\rho = 5/6$  states. Thus, the system displays a rich structure of the VCBS states for the trilayer system. As in the case of the bilayer system, the VCBS states are also incompressible. They result from the increased degrees of freedom associated with the interlayer hopping. The particle-hole symmetry of the trilayer system which can be deduced from the phase diagram is  $\mu/V = 1$ . This particle-hole symmetric  $\mu/V$  value is also analytically obtained from Eq.(A5), the details are given in the Appendix (A).

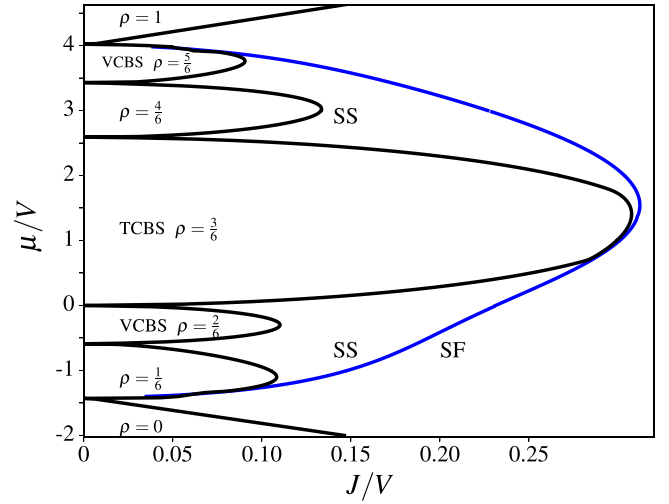


FIG. 11. Phase diagram for trilayer optical lattice in the  $J/V$ - $\mu/V$  plane for  $J'/V = 1$  and  $V'/V = -1$ . The black solid lines represent the phase boundaries between incompressible and compressible phases, and the blue lines indicate the phase boundaries between SS and SF phase, obtained numerically with  $2 \times 1 \times 3$  clusters in the CGMF method and with open boundary condition along  $z$  direction.

As  $J/V$  is increased, the system acquires higher intralayer hopping energy. This, then, leads to co-existence of diagonal and off-diagonal long range order in the system and makes the system compressible. The system is then in the supersolid phase. The supersolid phases envelopes the VCBS states, earlier similar results observed for the bilayered systems. For an  $n$ -layered system, we can generalize the VCBS states from  $\rho = 1/2n$  to  $\rho = 2n - 1/2n$ , excluding the  $\rho = n/2n = 1/2$  state. We thus observe that our results can be generalized for the multilayered systems. This generalization is evident from the states obtained for bi- and trilayer systems. It is to be emphasized that the trilayer system is the minimal one where the distinction between boundary and bulk layers is applicable. To avoid boundary effects and represent multilayer system with larger number of layers we used periodic boundary conditions. The choice of open boundary conditions, on the other hand, is not an appropriate one as the boundary effects can influence the quantum phases and corresponding phase diagrams.

To illustrate the boundary effects and its impact on the phase diagram, we compute the quantum phases and phase diagram with open boundary condition along  $z$  direction. However, with periodic boundary conditions along  $x$  and  $y$  directions. We obtain quantum phases similar to the periodic boundary condition along  $z$  direction. In general, as there is no hopping and interaction between the first and third layer, the basis states in Eqs. (20) and (21) do not have equal coefficients. For example, the state analogous to the  $|w_0\rangle_{p,q}$  is  $\frac{1}{2}(|100\rangle_{p,q} + \sqrt{2}|010\rangle_{p,q} + |001\rangle_{p,q})$  and it is independent of  $J'$  and  $V'$ . On the other hand, for the present case of  $V' = -J'$ , the  $|w_1\rangle_{p,q}$  state remains unchanged. However, this state is modified for other choices of  $J'$  and  $V'$ . The phase diagram of the trilayer system with open boundary condition is shown in Fig. 11. The phase diagram is not symmetric as observed in Fig. 10. There are also other qualitative differences like the

type of phases, phase boundaries and range of the chemical potential. Unlike the periodic boundary condition, we cannot obtain the analytical phase boundaries with the open boundary condition. The reason is that the homogeneity of the sublattice structures is essential for the perturbative analysis used in the analytical method.

## V. CONCLUSIONS

In conclusion, we have examined the quantum phases of the polarized dipolar atoms in multilayer optical lattices at zero and finite temperatures. The rich phase diagrams of the model display parameter domains for dimer (trimer) checkerboard solid and valence bond checkerboard solid phases for the bi-(tri-)layer lattice system. The interlayer attractive interaction is responsible for formation of the dimers (trimers), and the intralayer repulsion induces the in-plane checkerboard ordering. This stabilizes dimer (trimer) checkerboard solid phase for average occupancy  $\rho = 1/2$ . With the increase in interlayer hopping the dimers (trimers) break to form resonating valence bond like states. Then, the bilayer lattice can exhibit VCBS phases with average occupancies  $\rho = 1/4$  and  $3/4$ , respectively. Similarly, the trilayer lattice supports VCBS phases with  $\rho = 1/6, 2/6, 4/6$ , and  $5/6$ . These states are stabilized when  $J' > |V'|/2$ , and the corresponding lobes are enlarged with increasing interlayer hopping strength  $J'$ . On the contrary, the parameter domain of the dimer (trimer) checkerboard solid shrinks with increasing  $J'$ . In addition to the solid phases, the system also exhibits supersolid phases. In the weak and moderate interlayer hopping regime, this phase appear in the vicinity of both the DCBS and VCBS lobes. However, the domains envelope only the VCBS lobes for strong interlayer hopping, indicating the valence bond nature of the supersolid phase. With the inclusion of the thermal fluctuations, the quantum phases are observed to melt to a structured normal fluid, where the melting of the VCBS phase occurs at a lower temperature than the DCBS phase.

## ACKNOWLEDGMENTS

The results presented in the paper are based on the computations using Vikram-100, the 100TFLOP HPC Cluster at Physical Research Laboratory, Ahmedabad, India. S.B acknowledges the support by Quantum Science and Technology in Trento (Q@TN), Provincia Autonoma di Trento, and the ERC Starting Grant StrEnQTh (Project-ID 804305). SM acknowledges support from the DST, Govt. of India.

## APPENDIX A: PARTICLE-HOLE SYMMETRY

The particle-hole symmetry of the Hamiltonian in Eq. (2) can be seen by doing the particle hole transformation of the creation and annihilation operators. The following transformation is used

$$\begin{aligned}\hat{a}_{i,r}^\dagger &= \hat{b}_{i,r}, \\ \hat{a}_{i,r} &= \hat{b}_{i,r}^\dagger,\end{aligned}$$

where the operators  $\hat{a}_{i,r}$  and  $\hat{a}_{i,r}^\dagger$  are the hole annihilation and creation operators. The particle and the hole operators satisfy

the canonical anti-commutation relation

$$\begin{aligned}\{\hat{b}_{i,r}, \hat{b}_{i,r}^\dagger\} &= 1, \\ \{\hat{a}_{i,r}, \hat{a}_{i,r}^\dagger\} &= 1.\end{aligned}$$

With these expressions, the Hamiltonian in Eq. (2) can be rewritten as

$$\begin{aligned}\hat{H}_{\text{bi}} &= -J \sum_{\langle ij \rangle, r} (\hat{a}_{i,r} \hat{a}_{j,r}^\dagger + \text{H.c.}) - J' \sum_i (\hat{a}_{i,1} \hat{a}_{i,2}^\dagger + \text{H.c.}) \\ &+ V \sum_{\langle ij \rangle, r} \hat{a}_{i,r} \hat{a}_{i,r}^\dagger \hat{a}_{j,r} \hat{a}_{j,r}^\dagger + V' \sum_i \hat{a}_{i,1} \hat{a}_{i,1}^\dagger \hat{a}_{i,2} \hat{a}_{i,2}^\dagger \\ &- \mu \sum_{i,r} \hat{a}_{i,r} \hat{a}_{i,r}^\dagger.\end{aligned}\quad (\text{A1})$$

This can be further simplified as

$$\begin{aligned}\hat{H}_{\text{bi}} &= -J \sum_{\langle ij \rangle, r} (\hat{a}_{j,r}^\dagger \hat{a}_{i,r} + \text{H.c.}) - J' \sum_i (\hat{a}_{i,2}^\dagger \hat{a}_{i,1} + \text{H.c.}) \\ &+ V \sum_{\langle ij \rangle, r} (1 - \hat{n}_{i,r})(1 - \hat{n}_{j,r}) \\ &+ V' \sum_i (1 - \hat{n}_{i,1})(1 - \hat{n}_{i,2}) - \mu \sum_{i,r} (1 - \hat{n}_{i,r}),\end{aligned}\quad (\text{A2})$$

where the hole number operator is  $\hat{n}_{i,r} = \hat{a}_{i,r}^\dagger \hat{a}_{i,r}$ .

$$\begin{aligned}\hat{H}_{\text{bi}} &= -J \sum_{\langle ij \rangle, r} (\hat{a}_{j,r}^\dagger \hat{a}_{i,r} + \text{H.c.}) - J' \sum_i (\hat{a}_{i,2}^\dagger \hat{a}_{i,1} + \text{H.c.}) \\ &+ V \sum_{\langle ij \rangle, r} (\hat{n}_{i,r} \hat{n}_{j,r} - \hat{n}_{j,r} - \hat{n}_{i,r} + 1) \\ &+ V' \sum_i (\hat{n}_{i,1} \hat{n}_{i,2} - \hat{n}_{i,1} - \hat{n}_{i,2} + 1) - \mu \sum_{i,r} (1 - \hat{n}_{i,r}),\end{aligned}\quad (\text{A3})$$

$$\begin{aligned}\hat{H}_{\text{bi}} &= -J \sum_{\langle ij \rangle, r} (\hat{a}_{j,r}^\dagger \hat{a}_{i,r} + \text{H.c.}) - J' \sum_i (\hat{a}_{i,2}^\dagger \hat{a}_{i,1} + \text{H.c.}) \\ &+ V \sum_{\langle ij \rangle, r} \hat{n}_{i,r} \hat{n}_{j,r} - zV \sum_{i,r} \hat{n}_{i,r} \\ &+ V' \sum_i \hat{n}_{i,1} \hat{n}_{i,2} - V' \sum_{i,r} \hat{n}_{i,r} + \mu \sum_{i,r} \hat{n}_{i,r} \\ &= -J \sum_{\langle ij \rangle, r} (\hat{a}_{j,r}^\dagger \hat{a}_{i,r} + \text{H.c.}) - J' \sum_i (\hat{a}_{i,2}^\dagger \hat{a}_{i,1} + \text{H.c.}) \\ &+ V \sum_{\langle ij \rangle, r} \hat{n}_{i,r} \hat{n}_{j,r} + V' \sum_i \hat{n}_{i,1} \hat{n}_{i,2} - \tilde{\mu} \sum_{i,r} \hat{n}_{i,r},\end{aligned}$$

where  $\tilde{\mu} = (-\mu + zV + V')$ .

Particle hole symmetry point is

$$\begin{aligned}\mu &= \tilde{\mu} \\ \Rightarrow \mu &= -\mu + zV + V' \\ \Rightarrow \mu &= \left( \frac{zV + V'}{2} \right).\end{aligned}\quad (\text{A4})$$

Similarly, for a multilayer system, the particle-hole symmetry point is

$$\mu = \left( \frac{zV + 2V'}{2} \right).\quad (\text{A5})$$

This result is obtained after employing the periodic boundary condition along  $z$  direction.

## APPENDIX B: TRILAYER PHASE BOUNDARY

We present the derivation of the analytical phase boundaries of the quantum phases of the trilayer optical lattice. We first derive the phase boundary separating the TCBS  $\rho = 1/2$  domain from the compressible phase.

### 1. TCBS phase boundary

As discussed for the phase boundary of the DCBS phase, we first write the site-decoupled unperturbed Hamiltonian for trilayer optical lattice as

$$\hat{h}_{p,q}^{(0)} = \sum_{r=1}^3 \hat{n}_{p,q,r} (V' n_{p,q,r+1} + V \bar{n}_{p,q,r} - \mu). \quad (\text{B1})$$

It has to be understood that the  $r + 1$  in the above equation is considered with modulo 3, so that we have interaction between the first and third layers. The unperturbed energies corresponding to the eigenstates  $|n_1^r, n_2^r, n_3^r\rangle$  of the unperturbed Hamiltonian ( $r = \{A, B\}$ ) are

$$E_{n_1^A n_2^A n_3^A}^A = V' (n_1^A n_2^A + n_2^A n_3^A + n_3^A n_1^A) + \sum_{r=1}^3 (4V n_r^A n_r^B - \mu n_r^A), \quad (\text{B2})$$

for  $(p, q) \in A$ , and

$$E_{n_1^B n_2^B n_3^B}^B = V' (n_1^B n_2^B + n_2^B n_3^B + n_3^B n_1^B) + \sum_{r=1}^3 (4V n_r^B n_r^A - \mu n_r^B), \quad (\text{B3})$$

for  $(p, q) \in B$ . The perturbation Hamiltonian is

$$\begin{aligned} \hat{T}^A &= -4J \sum_{r=1}^3 \phi_r^B (\hat{b}_r^A + \hat{b}_r^{A\dagger}) - 2J' \sum_{r=1}^3 \phi_{r+1}^A (\hat{b}_r^A + \hat{b}_r^{A\dagger}), \\ \hat{T}^B &= -4J \sum_{r=1}^3 \phi_r^A (\hat{b}_r^B + \hat{b}_r^{B\dagger}) - 2J' \sum_{r=1}^3 \phi_{r+1}^B (\hat{b}_r^B + \hat{b}_r^{B\dagger}). \end{aligned}$$

The TCBS state, given by Eq. (22), has occupancies as  $(n_1^A, n_2^A, n_3^A) = (1, 1, 1)$  and  $(n_1^B, n_2^B, n_3^B) = (0, 0, 0)$ . Then, the perturbed ground state for sublattice A, similar to the one in

Eq. (36), is

$$|\chi^A\rangle = |111\rangle^A + \sum_{m_1^A, m_2^A, m_3^A} \frac{(m_1^A m_2^A m_3^A | \hat{T}^A | 111\rangle^A)}{(E_{111}^A - E_{m_1 m_2 m_3}^A)} |m_1^A m_2^A m_3^A\rangle, \quad (\text{B4})$$

where  $(m_1^A, m_2^A, m_3^A) \neq (1, 1, 1)$ . Substituting the perturbation Hamiltonian  $\hat{T}^A$  in the previous equation, we obtain

$$\begin{aligned} |\chi^A\rangle &= |111\rangle^A + (-4J\phi_B - 2J'\phi_A) \\ &\times \left[ \frac{|011\rangle^A}{(E_{111}^A - E_{011}^A)} + \frac{|101\rangle^A}{(E_{111}^A - E_{101}^A)} + \frac{|110\rangle^A}{(E_{111}^A - E_{110}^A)} \right]. \end{aligned} \quad (\text{B5})$$

And similarly, the perturbed state for sublattice B is

$$\begin{aligned} |\chi^B\rangle &= |000\rangle^B + (-4J\phi_A - 2J'\phi_B) \\ &\times \left[ \frac{|100\rangle^B}{(E_{000}^B - E_{100}^B)} + \frac{|010\rangle^B}{(E_{000}^B - E_{010}^B)} + \frac{|001\rangle^B}{(E_{000}^B - E_{001}^B)} \right]. \end{aligned} \quad (\text{B6})$$

Like in the bilayer case, we have assumed that  $\phi_r^A = \phi^A$  and  $\phi_r^B = \phi^B$  for all values of  $r$ . We can substitute the energy difference denominators by calculating the energies, using Eqs. (B2) and (B3). Then, we calculate the order parameter for sublattice A and B to get

$$\phi^A = -\frac{4J\phi^B}{2V' - \mu + 2J'} \quad (\text{B7})$$

and

$$\phi^B = -\frac{4J\phi^A}{\mu - 4V + 2J'}. \quad (\text{B8})$$

Solving these two equations simultaneously, and taking the limit  $\{\phi^A, \phi^B\} \rightarrow 0^+$ , we get the phase boundary separating the TCBS phase from the compressible phase, given in Eq. (41).

### 2. VCBS phase boundary

We first discuss the derivation of the phase boundary between the VCBS  $\rho = 1/6$  phase and the compressible phase. The unperturbed local Hamiltonian for sublattice A is

$$\mathcal{H}_A^{(0)} = -J' \sum_{r=1}^3 (\hat{b}_{p,q,r}^\dagger \hat{b}_{p,q,r+1} + \text{H.c.}) + V' \sum_{r=1}^3 \hat{n}_{p,q,r} \hat{n}_{p,q,r+1} + \sum_{r=1}^3 (V \hat{n}_{p,q,r} \bar{n}_{p,q,r} - \mu \hat{n}_{p,q,r}). \quad (\text{B9})$$

The eigenstates of this unperturbed Hamiltonian are

$$\begin{aligned} \left\{ |000\rangle, |111\rangle, |w_0\rangle = \frac{1}{\sqrt{3}} (|001\rangle + |010\rangle + |100\rangle), \right. \\ |\alpha^1\rangle = \frac{1}{\sqrt{2}} (|001\rangle - |100\rangle), \quad |\beta^1\rangle = \frac{1}{\sqrt{2}} (|010\rangle - |100\rangle), \\ |w_1\rangle = \frac{1}{\sqrt{3}} (|011\rangle + |110\rangle + |101\rangle), \\ \left. |\alpha^2\rangle = \frac{1}{\sqrt{2}} (|011\rangle - |110\rangle), \quad |\beta^2\rangle = \frac{1}{\sqrt{2}} (|101\rangle - |110\rangle) \right\}. \end{aligned}$$

The perturbation Hamiltonian consists of only the intralayer hopping terms and has a similar form as that of Eq. (35). For the VCBS  $\rho = 1/6$  phase, the  $|w_0\rangle$  state is present at sublattice A. The first order correction to the wave function at sublattice A is then given by

$$|\chi^A\rangle = |w_0\rangle^A + \sum_{\Gamma \neq w_0} \frac{\langle \Gamma | \hat{T}^A | w_0 \rangle^A}{(E_{w_0}^A - E_{\Gamma}^A)} |\Gamma\rangle,$$

where the state  $|\Gamma\rangle$  in the summation is chosen from the set of the eigenstates stated previously. Then, with the substitution of the perturbing Hamiltonian, and simplifying steps, we obtain the expression for the perturbed state as

$$|\chi^A\rangle = |w_0\rangle^A - 4J\varphi^B \left( \frac{\sqrt{3}}{-\mu - 2J'} |000\rangle + \frac{2}{\mu - V'} |w_1\rangle \right). \quad (\text{B10})$$

The  $\varphi_A = \langle \chi^A | \hat{b}^A | \chi^A \rangle$  is then given as

$$\varphi^A = -4J\varphi^B \left( \frac{1}{-\mu - 2J'} + \frac{4}{3(\mu - 4V')} \right). \quad (\text{B11})$$

Since the state on the sublattice B is  $|000\rangle$  for VCBS  $\rho = 1/6$  phase, we can use the expression given in Eq. (B8). Then solving for  $\varphi^A$  and  $\varphi^B$  simultaneously and taking the limit  $\{\varphi^A, \varphi^B\} \rightarrow 0^+$ , we get Eq. (42). A similar analysis can be performed for obtaining the phase boundary of the VCBS  $\rho = 2/6$  and the compressible phase. The particle-hole symmetry can be exploited to obtain the phase boundaries of the VCBS  $\rho = 4/6$  and  $5/6$  states. We can substitute  $\mu \rightarrow -\mu + zV + 2V'$  in the phase boundaries of VCBS  $\rho = 1/6$  and  $2/6$  states, to get the phase boundaries of VCBS  $\rho = 5/6$  and  $4/6$  states.

- 
- [1] M. Greiner, O. Mandel, T. Esslinger, T. W. Hänsch, and I. Bloch, *Nature (London)* **415**, 39 (2002).
- [2] M. Greiner, O. Mandel, T. W. Hänsch, and I. Bloch, *Nature (London)* **419**, 51 (2002).
- [3] T. Stöferle, H. Moritz, C. Schori, M. Köhl, and T. Esslinger, *Phys. Rev. Lett.* **92**, 130403 (2004).
- [4] S. Fölling, A. Widera, T. Müller, F. Gerbier, and I. Bloch, *Phys. Rev. Lett.* **97**, 060403 (2006).
- [5] I. B. Spielman, W. D. Phillips, and J. V. Porto, *Phys. Rev. Lett.* **98**, 080404 (2007).
- [6] S. Baier, M. J. Mark, D. Petter, K. Aikawa, L. Chomaz, Z. Cai, M. Baranov, P. Zoller, and F. Ferlaino, *Science* **352**, 201 (2016).
- [7] D. Jaksch and P. Zoller, *Ann. Phys.* **315**, 52 (2005), special Issue.
- [8] I. Bloch, J. Dalibard, and W. Zwerger, *Rev. Mod. Phys.* **80**, 885 (2008).
- [9] I. Bloch, *Nature (London)* **453**, 1016 (2008).
- [10] M. Lewenstein, A. Sanpera, V. Ahufinger, B. Damski, A. Sen(De), and U. Sen, *Adv. Phys.* **56**, 243 (2007).
- [11] C. Gross and I. Bloch, *Science* **357**, 995 (2017).
- [12] D. Jaksch, C. Bruder, J. I. Cirac, C. W. Gardiner, and P. Zoller, *Phys. Rev. Lett.* **81**, 3108 (1998).
- [13] K. Góral, L. Santos, and M. Lewenstein, *Phys. Rev. Lett.* **88**, 170406 (2002).
- [14] I. Danshita and C. A. R. Sá de Melo, *Phys. Rev. Lett.* **103**, 225301 (2009).
- [15] S. Yi, T. Li, and C. P. Sun, *Phys. Rev. Lett.* **98**, 260405 (2007).
- [16] C. Zhang, A. Safavi-Naini, A. M. Rey, and B. Capogrosso-Sansone, *New J. Phys.* **17**, 123014 (2015).
- [17] S. Bandyopadhyay, R. Bai, S. Pal, K. Suthar, R. Nath, and D. Angom, *Phys. Rev. A* **100**, 053623 (2019).
- [18] S. Pal, R. Bai, S. Bandyopadhyay, K. Suthar, and D. Angom, *Phys. Rev. A* **99**, 053610 (2019).
- [19] K. Suthar, H. Sable, R. Bai, S. Bandyopadhyay, S. Pal, and D. Angom, *Phys. Rev. A* **102**, 013320 (2020).
- [20] K. Suthar, R. Kraus, H. Sable, D. Angom, G. Morigi, and J. Zakrzewski, *Phys. Rev. B* **102**, 214503 (2020).
- [21] K. Suthar, A. Roy, and D. Angom, *Phys. Rev. A* **91**, 043615 (2015).
- [22] K. Suthar and D. Angom, *Phys. Rev. A* **93**, 063608 (2016).
- [23] K. Suthar and D. Angom, *Phys. Rev. A* **95**, 043602 (2017).
- [24] K. V. Krutitsky, J. Larson, and M. Lewenstein, *Phys. Rev. A* **82**, 033618 (2010).
- [25] K. V. Krutitsky and P. Navez, *Phys. Rev. A* **84**, 033602 (2011).
- [26] T. Saito, I. Danshita, T. Ozaki, and T. Nikuni, *Phys. Rev. A* **86**, 023623 (2012).
- [27] D. Chen, M. White, C. Borries, and B. DeMarco, *Phys. Rev. Lett.* **106**, 235304 (2011).
- [28] S. Braun, M. Friesdorf, S. S. Hodgman, M. Schreiber, J. P. Ronzheimer, A. Riera, M. del Rey, I. Bloch, J. Eisert, and U. Schneider, *Proc. Natl. Acad. Sci.* **112**, 3641 (2015).
- [29] K. Shimizu, Y. Kuno, T. Hirano, and I. Ichinose, *Phys. Rev. A* **97**, 033626 (2018).
- [30] K. Shimizu, T. Hirano, J. Park, Y. Kuno, and I. Ichinose, *Phys. Rev. A* **98**, 063603 (2018).
- [31] K. Shimizu, T. Hirano, J. Park, Y. Kuno, and I. Ichinose, *New J. Phys.* **20**, 083006 (2018).
- [32] Y. Zhou, Y. Li, R. Nath, and W. Li, *Phys. Rev. A* **101**, 013427 (2020).
- [33] H. Sable, D. Gaur, S. Bandyopadhyay, R. Nath, and D. Angom, *arXiv:2106.01725*.
- [34] A. M. Kaufman, M. E. Tai, A. Lukin, M. Rispoli, R. Schittko, P. M. Preiss, and M. Greiner, *Science* **353**, 794 (2016).
- [35] A. Bohrt, C. B. Mendl, M. Endres, and M. Knap, *New J. Phys.* **19**, 063001 (2017).
- [36] P. Sierant, D. Delande, and J. Zakrzewski, *Phys. Rev. A* **95**, 021601(R) (2017).
- [37] P. Sierant and J. Zakrzewski, *New J. Phys.* **20**, 043032 (2018).
- [38] T. Tomita, S. Nakajima, I. Danshita, Y. Takasu, and Y. Takahashi, *Sci. Adv.* **3**, e1701513 (2017).
- [39] A. Roy and K. Saha, *New J. Phys.* **21**, 103050 (2019).
- [40] M. P. A. Fisher, P. B. Weichman, G. Grinstein, and D. S. Fisher, *Phys. Rev. B* **40**, 546 (1989).
- [41] J. Hubbard, *Proc. Royal Soc. A* **276**, 238 (1963).
- [42] V. W. Scarola and S. Das Sarma, *Phys. Rev. Lett.* **95**, 033003 (2005).

- [43] D. L. Kovrizhin, G. V. Pai, and S. Sinha, *Europhys. Lett.* **72**, 162 (2005).
- [44] P. Sengupta, L. P. Pryadko, F. Alet, M. Troyer, and G. Schmid, *Phys. Rev. Lett.* **94**, 207202 (2005).
- [45] G. Mazzarella, S. M. Giampaolo, and F. Illuminati, *Phys. Rev. A* **73**, 013625 (2006).
- [46] M. Iskin, *Phys. Rev. A* **83**, 051606(R) (2011).
- [47] O. Dutta, M. Gajda, P. Hauke, M. Lewenstein, D.-S. Lühmann, B. A. Malomed, T. Sowiński, and J. Zakrzewski, *Rep. Prog. Phys.* **78**, 066001 (2015).
- [48] M. Boninsegni and N. V. Prokof'ev, *Rev. Mod. Phys.* **84**, 759 (2012).
- [49] C. Menotti, C. Trefzger, and M. Lewenstein, *Phys. Rev. Lett.* **98**, 235301 (2007).
- [50] H.-K. Wu and W.-L. Tu, *Phys. Rev. A* **102**, 053306 (2020).
- [51] Y. Cao, V. Fatemi, S. Fang, K. Watanabe, T. Taniguchi, E. Kaxiras, and P. Jarillo-Herrero, *Nature (London)* **556**, 43 (2018), article.
- [52] Y. Cao, V. Fatemi, A. Demir, S. Fang, S. L. Tomarken, J. Y. Luo, J. D. Sanchez-Yamagishi, K. Watanabe, T. Taniguchi, E. Kaxiras, R. C. Ashoori, and P. Jarillo-Herrero, *Nature (London)* **556**, 80 (2018).
- [53] B. Lian, Z. Wang, and B. A. Bernevig, *Phys. Rev. Lett.* **122**, 257002 (2019).
- [54] F. Wu, A. H. MacDonald, and I. Martin, *Phys. Rev. Lett.* **121**, 257001 (2018).
- [55] J. González and T. Stauber, *Phys. Rev. Lett.* **122**, 026801 (2019).
- [56] A. González-Tudela and J. I. Cirac, *Phys. Rev. A* **100**, 053604 (2019).
- [57] J. M. Pizarro, M. J. Calderón, and E. Bascones, *J. Phys. Commun.* **3**, 035024 (2019).
- [58] P. S. Mahapatra, B. Ghawri, M. Garg, S. Mandal, K. Watanabe, T. Taniguchi, M. Jain, S. Mukerjee, and A. Ghosh, *Phys. Rev. Lett.* **125**, 226802 (2020).
- [59] X.-W. Luo and C. Zhang, *Phys. Rev. Lett.* **126**, 103201 (2021).
- [60] A. Macia, G. E. Astrakharchik, F. Mazzanti, S. Giorgini, and J. Boronat, *Phys. Rev. A* **90**, 043623 (2014).
- [61] F. Cinti, D.-W. Wang, and M. Boninsegni, *Phys. Rev. A* **95**, 023622 (2017).
- [62] C. Trefzger, C. Menotti, and M. Lewenstein, *Phys. Rev. Lett.* **103**, 035304 (2009).
- [63] A. Safavi-Naini, Ş. G. Söyler, G. Pupillo, H. R. Sadeghpour, and B. Capogrosso-Sansone, *New J. Phys.* **15**, 013036 (2013).
- [64] K.-K. Ng, *Phys. Rev. B* **91**, 054516 (2015).
- [65] P. Buonsante, V. Penna, and A. Vezzani, *Phys. Rev. A* **70**, 061603(R) (2004).
- [66] D. Yamamoto, *Phys. Rev. B* **79**, 144427 (2009).
- [67] P. Pisarski, R. M. Jones, and R. J. Gooding, *Phys. Rev. A* **83**, 053608 (2011).
- [68] T. McIntosh, P. Pisarski, R. J. Gooding, and E. Zaremba, *Phys. Rev. A* **86**, 013623 (2012).
- [69] D.-S. Lühmann, *Phys. Rev. A* **87**, 043619 (2013).
- [70] D. van Oosten, P. van der Straten, and H. T. C. Stoof, *Phys. Rev. A* **63**, 053601 (2001).
- [71] M. Iskin and J. K. Freericks, *Phys. Rev. A* **79**, 053634 (2009).
- [72] R. Bai, D. Gaur, H. Sable, S. Bandyopadhyay, K. Suthar, and D. Angom, *Phys. Rev. A* **102**, 043309 (2020).
- [73] P. M. Preiss, R. Ma, M. E. Tai, J. Simon, and M. Greiner, *Phys. Rev. A* **91**, 041602(R) (2015).
- [74] J. Koepsell, S. Hirthe, D. Bourgund, P. Sompet, J. Vijayan, G. Salomon, C. Gross, and I. Bloch, *Phys. Rev. Lett.* **125**, 010403 (2020).
- [75] Z. Meng, L. Wang, W. Han, F. Liu, K. Wen, C. Gao, P. Wang, C. Chin, and J. Zhang, *arXiv:2110.00149* (2021).
- [76] T. Sowiński, O. Dutta, P. Hauke, L. Tagliacozzo, and M. Lewenstein, *Phys. Rev. Lett.* **108**, 115301 (2012).
- [77] J. Fraxanet, D. González-Cuadra, T. Pfau, M. Lewenstein, T. Langen, and L. Barbiero, *Phys. Rev. Lett.* **128**, 043402 (2022).
- [78] Y. Kuno and Y. Hatsugai, *Phys. Rev. B* **104**, 125146 (2021).
- [79] S. Stumper and J. Okamoto, *Phys. Rev. A* **101**, 063626 (2020).
- [80] D. Rossini and R. Fazio, *New J. Phys.* **14**, 065012 (2012).
- [81] E. Berg, E. G. Dalla Torre, T. Giamarchi, and E. Altman, *Phys. Rev. B* **77**, 245119 (2008).
- [82] D. S. Rokhsar and B. G. Kotliar, *Phys. Rev. B* **44**, 10328 (1991).
- [83] K. Sheshadri, H. R. Krishnamurthy, R. Pandit, and T. V. Ramakrishnan, *Europhys. Lett.* **22**, 257 (1993).
- [84] R. Bai, S. Bandyopadhyay, S. Pal, K. Suthar, and D. Angom, *Phys. Rev. A* **98**, 023606 (2018).
- [85] M. Malakar, S. Ray, S. Sinha, and D. Angom, *Phys. Rev. B* **102**, 184515 (2020).
- [86] W. Dür, G. Vidal, and J. I. Cirac, *Phys. Rev. A* **62**, 062314 (2000).
- [87] A. Safavi-Naini, J. von Stecher, B. Capogrosso-Sansone, and S. T. Rittenhouse, *Phys. Rev. Lett.* **109**, 135302 (2012).
- [88] K. W. Mahmud, E. N. Duchon, Y. Kato, N. Kawashima, R. T. Scalettar, and N. Trivedi, *Phys. Rev. B* **84**, 054302 (2011).
- [89] S. Fang, C.-M. Chung, P. N. Ma, P. Chen, and D.-W. Wang, *Phys. Rev. A* **83**, 031605(R) (2011).
- [90] L. de Forges de Parny, F. Hébert, V. G. Rousseau, and G. G. Batrouni, *Eur. Phys. J. B* **85**, 169 (2012).
- [91] M. Puschmann, J. C. Getelina, J. A. Hoyos, and T. Vojta, *Ann. Phys.* **435**, 168526 (2021), special Issue on Localisation 2020.